Integrating Deep Learning and Multi-Objective Optimization for Floodwater Utilization: A Coordinated Surface Water-Groundwater Regulation Framework for Groundwater Recovery

Libin Zhang[a], Yonggen Zhang[b]*, Jianzhu Li[a], Shaowei Lian[c], Xinwang Li[d], Ping Feng[a], Lutz Weihermüller[e]

[a] State Key Laboratory of Hydraulic Engineering Intelligent Construction and Operation, Tianjin University, Tianjin 300072, China

[b] Institute of Surface-Earth System Science, School of Earth System Science, Tianjin University, Tianjin 300072, China

[c] Hebei Provincial Hydrologic Survey and Research Center, Shijiazhuang 050051, China

[d] Hebei Institute of Water Science (Hebei province dam safety technology center, Hebei province levee sluice technology center), Shijiazhuang 050051, China

[e] Agrosphere Institute IBG-3, Forschungszentrum Jülich GmbH, Jülich, 52428, Germany

*Correspondence to: Yonggen Zhang (ygzhang@tju.edu.cn)

Abstract: Climate change has exacerbated global droughts and floods, further disrupted the uneven temporal and spatial distribution of water resources, and therefore, poses a significant challenge to water resource management. Flood utilization, converting floodwater from hazard to valuable resource, is a key solution to this challenge. However, existing flood utilization strategies predominantly focus on surface water management through reservoir operations, overlooking integrated optimization with groundwater systems, particularly the challenges of coupling physical models with multi-objective algorithms for groundwater recovery. Here, by ensuring ecological flow and downstream flood safety, a multi-objective optimization framework employing deep learning was developed to integrate flood control, water storage, and groundwater recovery. Reservoir operations were optimized through multi-scenario simulations, and a 3D groundwater numerical model was employed to assess the impact of managed aquifer recharge (MAR) using floodwater on groundwater recovery. Results for the 2023 flood season (June to September) showed that, increasing the flood limited water level (FLWL) reduced average reservoir flood risk and water scarcity by 84.9% and 61.9%, respectively, while weakening their inverse relationship. This indicates that raising FLWL improves individual objectives and reduces conflicts for balanced optimization. Maintaining continuous ecological river flow promoted groundwater recovery despite reduced total river discharge. MAR at 300 $m^3\ d^{-1}$ achieved effective groundwater recovery in 17.6% of the study area with a maximum of 0.46 m. Overall, this study presents a novel framework coupling deep learning, multi-objective optimization, and 3D groundwater modeling, enabling optimized surface water-groundwater regulation and enhanced floodwater utilization for groundwater recovery.

Keywords: Floodwater utilization; Deep learning; Groundwater recovery; Multi-objective optimization; Ecological flow; Managed aquifer recharge

1. Introduction

Global climate change is expected to intensify the hydrological cycle (Tabari, 2020), resulting in an increase in extreme precipitation events (Blöschl et al., 2017), leading to larger flood frequencies (Chagas et al., 2022), and posing significant challenges to water resource management, particularly in monsoon regions (Hirabayashi et al., 2013; Yang et al., 2023). This increase in flood intensity and frequency poses threats to ecosystems, economies, and human livelihoods (Bermúdez et al., 2021). In response to these challenges, innovative approaches such as floodwater utilization (FU) have been developed, which converts floodwater from a hazard into a valuable resource (Wang et al., 2023). This strategy has been increasingly adopted in integrated river basin management to balance water allocation (Li et al., 2021) and reservoir operation optimization to mitigate flood risks and water scarcity (Jiang et al., 2019), and enhance storage and recharge, while simultaneously controlling flood risks through strategic reservoir operations and flow regulation.

FU strategies typically involve drawing down reservoirs before the flood season to create additional storage capacity, capturing and storing excess floodwater during the flood season, and releasing the stored water for beneficial purposes such as irrigation and hydropower generation during the non-flood season (Wang et al., 2023). Maximizing reservoir operation benefits was achieved through multi-stage (Liu et al., 2015; Wei et al., 2022) or dynamic flood limited water level (FLWL) adjustments (Ding et al., 2023). Furthermore, the joint operation of multiple reservoirs (Jain et al., 2023) and the strategic use of flood retention areas (Bellu et al., 2016) have proven effective in optimizing FU. Where applied, these measures have reduced flood damage and enhanced floodwater utilization efficiency (Mateo et al., 2014).

However, while these FU strategies primarily focus on surface water management, research on the integrated optimization of groundwater systems, a fundamental component of the hydrological cycle (Irvine et al., 2024), remains limited. As critical hydrological components, groundwater resources undergo accelerated global depletion, threatening ecosystems and livelihoods (Jasechko et al., 2024). This is particularly severe in regions such as the North China Plain, which is one of the world's largest groundwater depression cones (Chen et al., 2020), highlighting the urgency of groundwater recovery efforts to sustain ecosystems and human activities. Consequently, effective groundwater recovery measures are imperative to counteract depletion and sustain ecosystems and livelihoods.

Accurate simulation of groundwater dynamics is essential for optimizing resource allocation in integrated water management (Haaf et al., 2023). Numerical simulation, the most widely used approach for modeling groundwater dynamics, has significantly contributed to analyzing spatial and temporal groundwater changes and quantifying the effects of various measures on groundwater dynamics (Condon et al., 2021). Roy et al. (2024) employed a MODFLOW model to determine the optimal groundwater recharge rate and to minimize groundwater decline. Lyu et al. (2025) employed an enhanced version of the SWAT-MODFLOW model to evaluate the effects of ecological recharge from reservoirs and reclaimed water releases on groundwater recovery. However, physical models might face limitations when integrated with optimization algorithms owing to their high computational intensity (Asher et al., 2015), as groundwater dynamics are influenced by multiple hydrogeological factors, including heterogeneity in subsurface hydraulic conductivities and extraction intensities (Kuang et al., 2024).

Recent advancements in deep learning, particularly Long Short-Term Memory (LSTM) networks, have yielded robust computational tools for groundwater prediction (Tripathy and Mishra, 2024). Due to their predictive accuracy (Cui et al., 2024) and potential for integration with optimization algorithms (He et al., 2022), LSTM networks have emerged as a preferred approach for analyzing nonlinear temporal features in hydrological time-series data (Hochreiter and Schmidhuber, 1997). However, analyzing the impacts of environmental factors on groundwater dynamics necessitates multi-step prediction approaches. To address error accumulation in such multi-step predictions, modifications to the LSTM architecture are necessary to minimize error propagation (Zhuang et al., 2023). The encoder-decoder LSTM architecture, which can effectively mitigate these issues by capturing temporal dependencies to improve prediction accuracy, has been extensively applied to temporal pattern recognition tasks, including natural language processing and activity forecasting (Deng et al., 2019). This architecture consists of encoder-decoder modules based on recurrent neural networks. The encoder transforms variable-length sequences into fixed-dimensional context vectors, while the decoder produces predictions by processing these vectors. Comparative analyses demonstrate that the encoder-decoder LSTM framework offers superior forecasting precision compared to conventional deep learning approaches (Wunsch et al., 2021; Xiang et al., 2020).

Despite many studies exploring floodwater utilization (FU) by reservoir regulation and the application of deep learning for groundwater level prediction, few studies have investigated the effects of using flood resources to promote groundwater recovery, by combining groundwater recovery with FU as a framework, leaving a critical gap in addressing the escalating global challenges of climate-driven floods, droughts, and widespread aquifer depletion. To address the limitations of prior studies, this study developed a framework, which embeds a deep learning model to predict groundwater levels, coupled with FU in multi-objective optimization. This framework also used a 3D groundwater numerical simulation to evaluate the spatial effects of managed aquifer recharge (MAR) using floodwater resources. The Lincheng Reservoir and its associated downstream groundwater depression cone in the North China Plain served as the testbed for this study.

The specific objectives of the study were: (1) to develop an encoder-decoder LSTM model for predicting groundwater levels and integrate it as a component of the objective function in multi-objective optimization; (2) to establish a multi-objective optimization framework that balances flood control, water storage, and groundwater recovery under constraints of ecological flows and flood safety; (3) to assess the effects of managed aquifer recharge (MAR) using floodwater on groundwater recovery through a 3D numerical model; (4) to evaluate the impacts of variations in deep learning hyperparameters (e.g., input sequence length) and MAR recharge rates on the framework's performance and optimization outcomes. The overall technical framework and workflow are illustrated in Figure 1. As depicted in Figure 1, the framework begins with data preparation in Step 1. Building on this, this study integrates deep learning into multi-objective optimization in Step 2 to jointly optimize flood control, water storage, and groundwater recovery. Subsequently, in Step 3, a numerical groundwater model (MODFLOW) is developed to quantify the effects of MAR on groundwater recovery, thereby transforming floodwater obtained from the previous step into a sustainable resource for groundwater restoration. In Step 4, this study discusses key factors, such as input sequence length and MAR rates, that influence the optimization outcomes and the potential risks involved. This approach provides a methodology for integrated water resource management in regions with groundwater overexploitation and intensive agricultural irrigation.

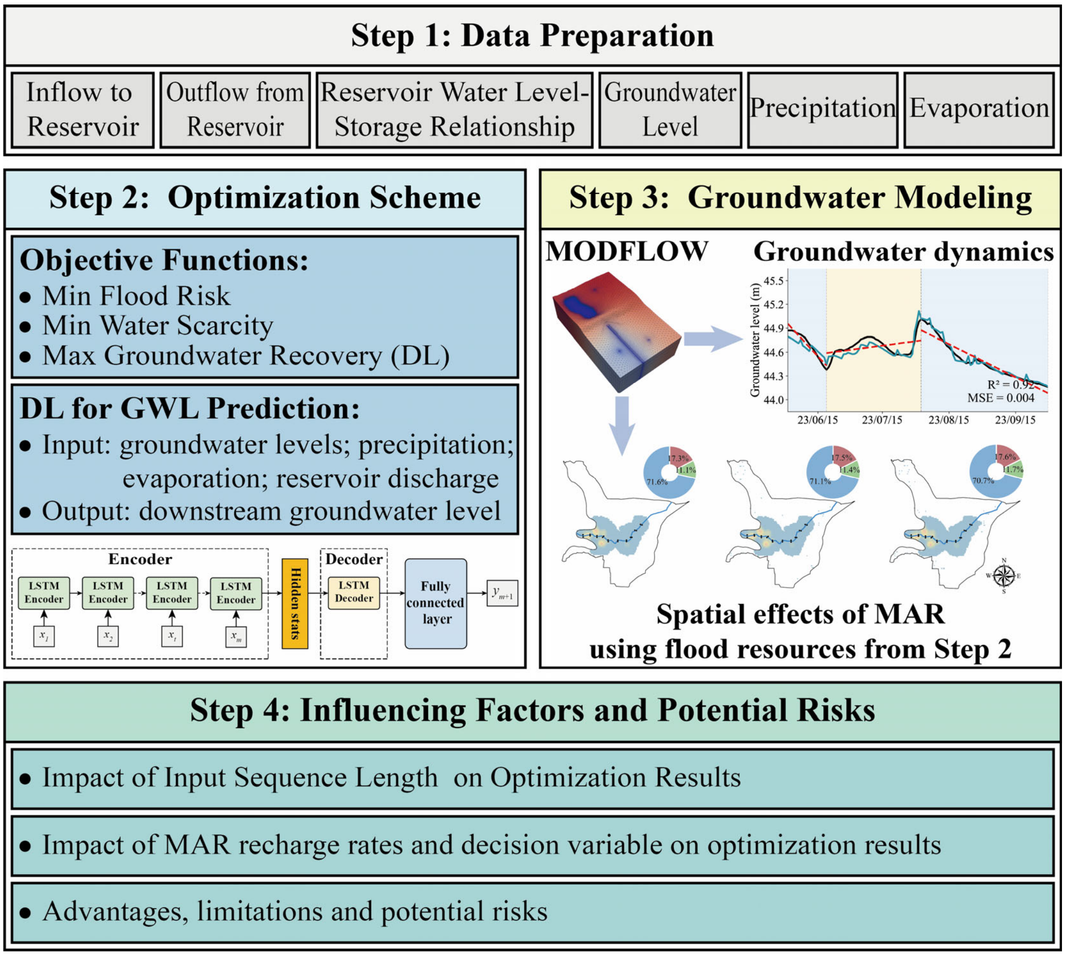

Figure 1. Schematic of the technical roadmap developed in this study, integrating

an optimization scheme for reservoir flood risk mitigation, water scarcity reduction, and groundwater recovery benefits. The MODFLOW model was used to evaluate the effectiveness of MAR, utilizing flood resources generated by the optimization scheme. The study also investigates key influencing factors and potential risks. Abbreviations in the figure: DL, deep learning; GWL, groundwater level; MAR, managed aquifer recharge.

2. Materials and Methods

2.1 Study Area

The Lincheng Reservoir is located in Xingtai City, Hebei Province, China and is part of the Ziya River system within the Haihe River basin (Figure 2a), which lies in a warm temperate continental monsoon climate zone. The average annual temperature ranges from 10 to 13°C, with significant variability in both inter-annual and intra-annual precipitation. Annual precipitation averages 490-600 mm, with 75-80% occurring during the summer months (July-August). Flood season precipitation primarily occurs in the form of high-intensity storms between late July and early August, resulting in an uneven temporal distribution of precipitation concentrated in short, intense periods.

The Lincheng Reservoir is primarily designed for flood control and water supply management. With a catchment area of 384 km^2, its key water levels include the dead storage level (112.0 m), the flood limited water level (FLWL, 120.48 m), and the normal storage level (125.5 m). The discharge from Lincheng Reservoir flows into the Zhi River, which then joins the Fuyang River (Figure 2b). The Zhi River basin is located within a representative shallow groundwater depression cone (GDC) in the North China Plain, i.e., the Ning-Bai-Long Cone (see the gray shaded area in Figure 2b), where groundwater levels have undergone significant decline. Since 1980, the development of the GDC has progressed through three primary stages (Figure 2c). From 1980 to 2014, the GDC expanded rapidly, with the average groundwater level experiencing a substantial decline of 30.3 m. Between 2014 and 2018, the expansion of the GDC slowed and the area-wide average groundwater level decreased again by 1.62 m. Since 2018, the ongoing implementation of over-extraction control measures has significantly reduced the expansion of the GDC, and as a consequence, the average groundwater level in the GDC had increased by 2.84 m in 2022 compared to 2018.

Considering these hydrogeological characteristics and the need for continued management of groundwater depletion, the study focuses on the Lincheng Reservoir and its downstream Zhi River basin, where optimized floodwater utilization offers an effective approach for coordinating multiple water management objectives, including flood control, water storage, ecological flow maintenance, and groundwater recovery.

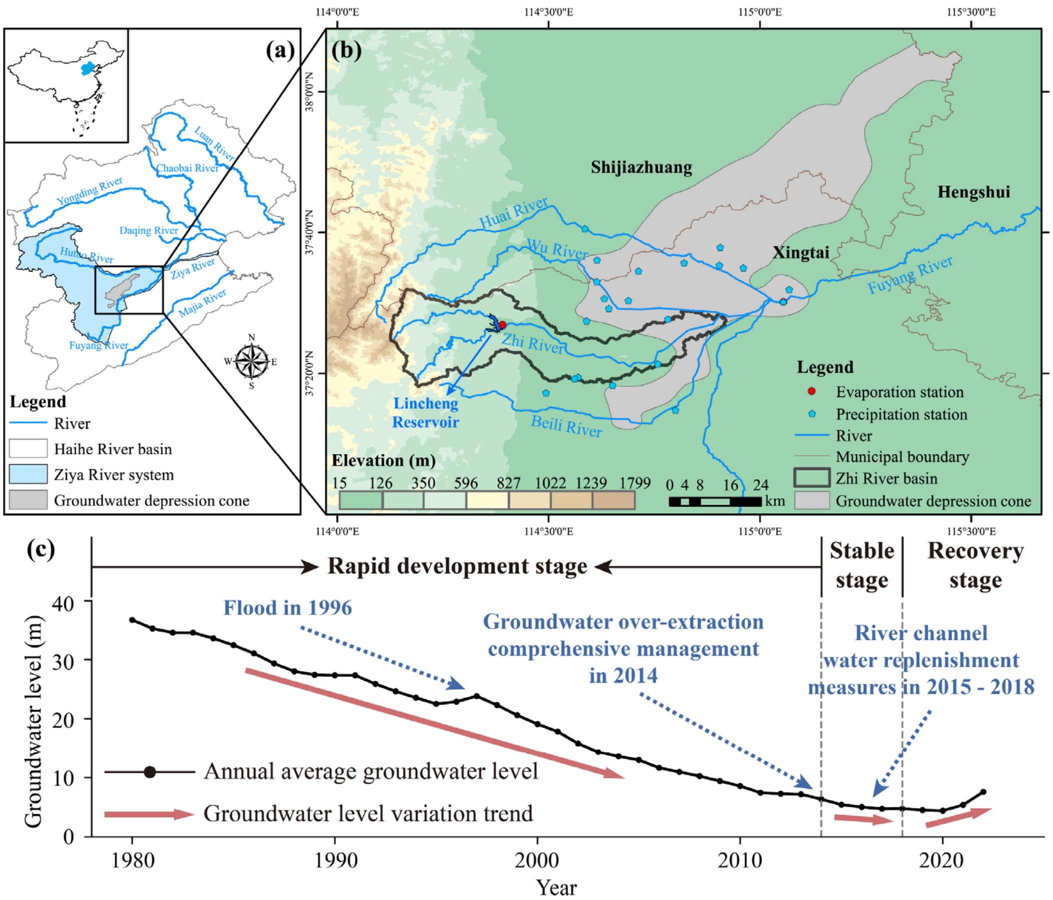

Figure 2. Overview of the study area: (a) Regional setting of the Haihe River basin and Ziya River system, with an inset map illustrating the geographical location of the Haihe River basin in China; (b) Hydrological characterization, including the Lincheng Reservoir, natural rivers, the groundwater depression cone, and hydrological monitoring stations; (c) Temporal evolution of the average groundwater level in the Ning-Bai-Long groundwater depression cone since 1980.

2.2 Data Sources

To support the integrated modeling framework for reservoir operations and groundwater dynamics in the Lincheng Reservoir and Zhi River basin, a comprehensive suite of hydrological, geological, and geospatial datasets was assembled from multiple authoritative sources. Daily inflow and outflow records for the reservoir, critical for simulating water balance and operational scenarios, were provided by the Xingtai Hydrological Survey and Research Center in Hebei Province, China. Meteorological monitoring data, including daily precipitation, potential evaporation, along with groundwater level observations, were sourced from the Hebei Provincial Hydrological Survey and Research Center to capture temporal variability in recharge and depletion patterns. Complementing these, high-resolution geospatial data, including a 90-m Digital Elevation Model (DEM) from the Geospatial Data Cloud (http://www.gscloud.cn) and 30-m land-use classifications from the GLC-FCS30 dataset (https://zenodo.org), enabled accurate delineation of the catchment topography and surface characteristics influencing runoff and infiltration processes. For the 3D groundwater numerical model, key hydrogeological parameters, including geological borehole logs, specific yields, hydraulic conductivities, infiltration coefficients, and groundwater extraction volumes, were obtained from the Ninth Geological Brigade of the Hebei Bureau of Geology and Mineral Resources.

2.3 Methods

2.3.1 Scenarios Setting of Flood Limited Water Level

To quantify the effects of changes in the flood limited water level (FLWL) on floodwater utilization (FU), this study developed three FLWL scenarios: (*a*) a fixed FLWL of 120.48 m, (*b*) a multi-stage FLWL, and (*c*) a fuzzy-segmentation FLWL, whereby the flood season was divided into pre-flood, main-flood, and post-flood seasons using fuzzy set theory (Mu et al., 2022). Detailed methods for flood season segmentation and fuzzy segmentation of FLWL determination are provided in the Supporting Information Text S1. Based on this segmentation, the FLWL for scenario (*b*) was set at 120.48 m for the pre-flood and main flood seasons and 123.48 m for the post-flood season. This configuration was recommended by the Hebei Provincial Water

Resources Department, based on their empirical assessments of historical flood patterns and reservoir safety. Nevertheless, alternative FLWL configurations are feasible within the proposed framework in this study. In scenario (*c*) the FLWL for each period was dynamically adjusted by linking the available flood control storage capacity to the varying reservoir levels across the pre-flood, main-flood, and post-flood seasons, as derived from historical precipitation patterns using fuzzy set theory. Detailed procedures and equations are provided in Supporting Information Text S1. Figure 3 illustrates the flood season segmentation and FLWL variations across scenarios.

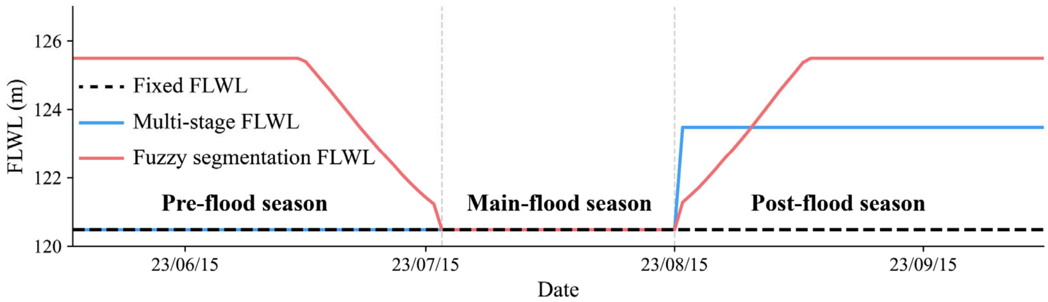

Figure 3. Variations in flood limited water level (FLWL) under different scenarios: the black dashed line represents fixed FLWL (Scenario *a*), the blue solid line indicates multi-stage FLWL (Scenario *b*), and the red solid line depicts fuzzy segmentation FLWL (Scenario *c*).

2.3.2 Groundwater Level Prediction Using encoder-decoder LSTM

This study adopted an encoder-decoder LSTM model, as its architecture serves as an extension of the LSTM and can better handle longer and more complex input sequences. In this architecture, the encoder processes a sequence of inputs (such as precipitation and evaporation) into a summarized representation that captures the essential temporal information (Sutskever et al., 2014), and then the decoder uses this information to predict the target variable (such as groundwater level). Compared to a simple LSTM, this design enables the model to capture long-term dependencies more effectively and reduces error accumulation during recursive forecasting.

The adopted encoder–decoder LSTM framework effectively represents the dynamic interaction between reservoir operations and groundwater responses. As depicted in Figure 4a, the encoder sequentially processes multiple hydrological and meteorological variables over several preceding time steps, capturing their temporal dependencies and compressing the information into a temporary state vector. At each time step t, the input vector x_t comprises historical groundwater levels, precipitation, potential evaporation, and reservoir discharge. After processing an input sequence of length m days, the encoder outputs the final hidden and cell states (h_m, c_m), which encapsulate the temporal dependencies of the sequence. The decoder then initializes with these states and produces the predicted groundwater level at the next time step (y_{m+1}) through a fully connected layer.

Both the encoder and decoder are composed of LSTM units that share the same internal gate structure and information-update mechanism. As shown in Figure 4b, the LSTM unit consists of three gates: the forget gate, input gate, and output gate. The forget gate (f_t) determines the proportion of the previous cell state c_{t-1} to discard, allowing the model to remove outdated information. Subsequently, the input gate (i_t) regulates the current external information (i.e., input x_t) and generates candidate cell state $\tilde{c}_t$ that represents potential new memory. The updated cell state c_t combines the past memory, weighted by the forget gate, with the candidate memory, weighted by the input gate. Finally, the output gate (o_t) selects features from the updated cell state c_t to produce hidden state h_t, which serves as the output to the next time step. Detailed equations and descriptions are provided in Supporting Information Text S2.

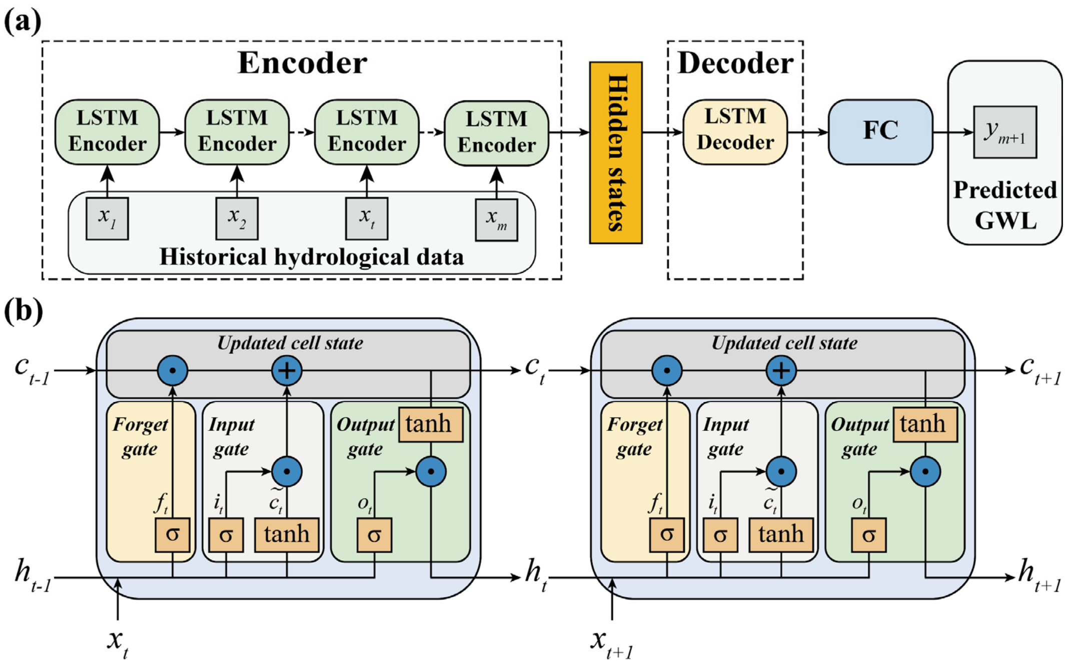

Figure 4. Model architecture: (a) Encoder–decoder LSTM framework for groundwater-level prediction. The encoder processes an input sequence of *m* time steps (x_1, x_2, …, x_m), where each x_t contains historical groundwater levels, precipitation, potential evaporation, and reservoir discharge. The decoder converts the encoded temporal information into the predicted downstream groundwater level (y_{m+1}). (b) Basic LSTM layer structure for the time step *t* to *t* + 1, with three essential gates including forget, input, and output gates that regulate the cell state update and control the information flow through the network.. Abbreviations in the figure: FC, fully connected layers; GWL, groundwater level.

As an important hyperparameter of encoder-decoder LSTM, temporal dependencies parameter (input sequence length) significantly influences model performance, particularly in capturing both short-term fluctuations and long-term trends in hydrological time series (Wunsch et al., 2021). To evaluate the model performance under varying input sequence length during the 2023 flood season, the dataset was partitioned into a training period (January 1, 2018 to May 31, 2023) and a testing period (June 1, 2023 to September 30, 2023). The methodological workflow comprised the following six phases:

1) Data preprocessing: normalization was applied to address dimensional discrepancies among heterogeneous features.

2) Input sequence length configuration: the length *m* was determined experimentally, ranging from 1 to 15 days, through parametric trials. This range was chosen to balance short-term and medium-term dependencies, ensuring that hydrological fluctuations can be effectively captured.

3) Network architecture: the encoder-decoder was coupled with the LSTM architecture. A fully connected layer converted decoder states into normalized predictions.

4) Model training: the Adam optimizer was used to minimize mean squared error (*MSE*) loss with a learning rate of 0.001. The training configuration included a batch size of 32 and a maximum of 200 epochs.

5) Post-processing: predictions were denormalized to derive GWL values.

6) Performance evaluation: prediction accuracy was quantified using the coefficient of determination ($R^2 \in [0,1]$) and mean squared error ($MSE \in [0,+\infty)$), with perfect predictions achieved when $R^2 = 1$ and $MSE = 0$.

2.3.3 Coupling Framework of Deep Learning and Multi-Objective Optimization

The coupled deep learning and multi-objective optimization framework was developed for the Lincheng Reservoir to optimize flood control, water storage, and groundwater recovery. This framework incorporates flood limited water level (FLWL) variations across operational scenarios to assess the impacts of strategies on multifunctional performance. The Non-dominated Sorting Genetic Algorithm II (NSGA-II) (Deb et al., 2002) was utilized to identify the Pareto frontier (i.e., the set of non-dominated solutions representing optimal trade-offs among competing objectives) under constraints.

2.3.3.1 Objective Functions

The developed multi-objective optimization framework incorporated the following objective functions:

The first is the reservoir flood risk during reservoir operation, which was quantified as the exceedance magnitude above FLWL. The corresponding objective was formulated to minimize the cumulative excessive flood damage as:

$$\min F_1 = \sum_{t=1}^{T} f_1^t \tag{1}$$

where T represents the total number of scheduling periods, and f_1^t is the relative flood exceedance in period t, defined as:

$$f_1^t = \begin{cases} (W_t - W_t^l)/W_t^l & W_t \geq W_t^l \\ 0 & W_t < W_t^l \end{cases} \tag{2}$$

where W_t and W_t^l represent the actual reservoir storage and the storage corresponding to the FLWL at the period t [L^3], respectively.

Water storage benefits were quantified by the ability of the reservoir to recover to the normal storage level after the flood season. The water scarcity objective aimed to minimize terminal storage deviation by:

$$\min F_2 = \frac{W_s - W_{t=T}}{W_s} \tag{3}$$

where W_s denotes the storage capacity at normal storage level [L^3] and $W_{t=T}$

represents the reservoir storage at the end of the regulation period [L^3].

Groundwater recovery benefits were evaluated through post-regulation groundwater level rise relative to baseline operations. The groundwater recovery objective maximized groundwater level elevation gain by:

$$\max F_3 = \frac{GWL - GWL_{base}}{GWL_{base}} \tag{4}$$

where GWL is the encoder-decoder LSTM predicted groundwater level under operational schemes [L], and GWL_{base} denotes the baseline groundwater level at the end of the flood season [L] without floodwater utilization.

2.3.3.2 Constraint Conditions

While minimizing the objective function the following constraints were used for the water balance:

$$W_t + I_{t+1} - R_{t+1} = W_{t+1} \tag{5}$$

where W_t and W_{t+1} are the reservoir storage volume at period *t* and *t*+1 [L^3]. I_{t+1} and R_{t+1} are the inflow and outflow volume at period *t*+1 [L^3], respectively.

The constraint on ecological flow was employed as:

$$Q_t \geq Q_t^{eco} \tag{6}$$

where Q_t^{eco} represents the downstream ecological flow at period *t* [L^3T^{-1}], calculated using the Tennant method (Tennant, 1976).

The constraint on downstream flood safety was defined as

$$Q_t \leq Q_{\max} \tag{7}$$

where $Q_{\max}$ denotes the maximum discharge for downstream flood protection [L^3T^{-1}]. $Q_{\max}$ was determined through hydrological frequency analysis using Pearson type

III distribution (Ji et al., 1984).

Finally, a constraint on reservoir storage was applied by:

$$W_{\min} \leq W_t \leq W_{\max} \tag{8}$$

where $W_{\min}$ and $W_{\max}$ are the reservoir storage correspond to dead storage level and normal storage level storage, respectively [L^3].

2.3.3.3 Optimization Algorithm Implementation

The 2023 extreme flood event in the Haihe River Basin was utilized as a case study to optimize daily reservoir operations, with the outflow-to-inflow ratio as the decision variable, which provides a normalized measure of reservoir release relative to incoming water volumes, thereby enabling flexible and scalable optimization across varying inflow conditions, while avoiding reliance on absolute outflow values that may fluctuate significantly with hydrological variability.

To balance the competing objectives of flood risk, water scarcity, and groundwater recovery using this decision variable, a multi-objective optimization model was developed and solved using the Non-dominated Sorting Genetic Algorithm II (NSGA-II) (Deb et al., 2002). NSGA-II enhances computational efficiency through fast non-dominated sorting and crowding distance mechanisms, while exhibiting robust performance across diverse engineering applications (Verma et al., 2021). Parameter configurations included a population size of 100, a maximum of 1,000 generations, a crossover probability of 0.9, and a mutation probability equal to the inverse of the number of decision variables.

Iterative optimization produced constrained discharge schemes, resulting in a non-dominated solution set across the three objectives defined. The projection pursuit method (Han et al., 2025) was utilized for Pareto front analysis. This method projects high-dimensional solutions onto a lower-dimensional subspace, facilitating quantitative analysis and decision-making, while mitigating the curse of dimensionality.

Additionally, Spearman's rank correlation coefficient was calculated for the objective function values to investigate relationships among the objectives. The Spearman's rank correlation coefficient (ρ) is calculated by:

$$\rho = 1 - \frac{6\sum d_i^2}{N(N^2 - 1)} \tag{9}$$

where d_i represents the difference between the ranks of corresponding values for each objective pair, and N denotes the number of observations.

2.3.4 Evaluation of Groundwater Recharge Measures

A three-dimensional groundwater numerical model was developed using the MODFLOW model to simulate the effectiveness of managed aquifer recharge (MAR) utilizing flood resources. Based on Darcy's law and the water balance principle, a system of partial differential equations was employed to simulate the groundwater flow numerically:

$$\begin{cases} \mu \dfrac{\partial h}{\partial t} = \dfrac{\partial}{\partial x}\left(K_x \dfrac{\partial h}{\partial x}\right) + \dfrac{\partial}{\partial y}\left(K_y \dfrac{\partial h}{\partial y}\right) + \dfrac{\partial}{\partial z}\left(K_z \dfrac{\partial h}{\partial z}\right) + \varepsilon \\ h(x,y,z,t)\big|_{t=0} = h_0 \\ h\big|_{\Gamma_1} = h_1(x,y,z,t) \\ K_n \dfrac{\partial h}{\partial \vec{n}}\Big|_{\Gamma_2} = q(x,y,z,t) \end{cases} \tag{10}$$

where K_x, K_y and K_z are the values of hydraulic conductivity [LT^{-1}] along the x, y and z coordinate axes in the simulation region Ω, h is the hydraulic head [L], ε is the source/sink term [LT^{-1}], μ is the specific yield, h_0 is the initial head [L], Γ_0 is the upper boundary condition, Γ_1 is the Dirichlet boundary condition, Γ_2 is the Neumann boundary condition, n is the outward normal direction of the Neumann boundary, q is the lateral flux per unit area and per unit time at the Neumann boundary [LT^{-1}], and K_n is the hydraulic conductivity in the normal direction at the boundary [LT^{-1}].

The simplification of boundary conditions was critical for the groundwater numerical simulation. Rivers can be simplified as Dirichlet conditions, while the boundaries between different hydrogeological zones can be simplified as Neumann conditions (flux boundary), with flow values calculated using Darcy's law based on multi-year groundwater level data. Therefore, as shown in Figure 5a, the northern Wu River and the southern Beili River were designated as Dirichlet boundary conditions. The western boundary, representing the boundary between the Taihang Mountains and the North China Plain, was designated as a Neumann boundary condition. The main channel of Zhi River was implemented as an internal river boundary condition.

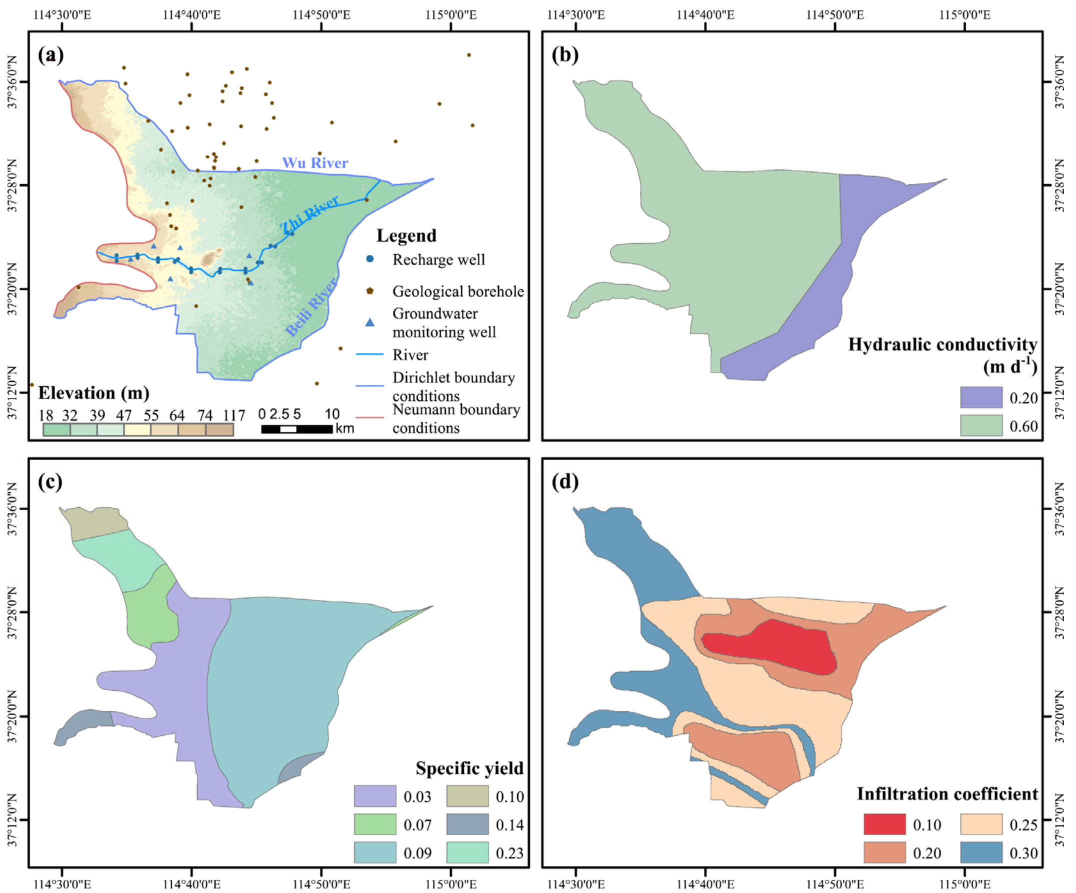

Figure 5. Overview of the 3D groundwater modeling area in the Zhi River basin for (a) boundary conditions and key features, including recharge wells (blue dots), geological boreholes (black dots), monitoring wells (blue triangle), with elevation contours in meters, and distributions of (b) hydraulic conductivity, (c) specific yield, and (d) infiltration coefficient.

Based on borehole data (Figure 5a), the aquifer system was vertically discretized into three layers: an unconfined aquifer (Layer 1), a semi-confined aquifer (Layer 2), and a confined aquifer (Layer 3). The absence of consistent impermeable layers between the unconfined and semi-confined aquifers results in a strong hydraulic connection. Given that the study area is located in a typical shallow groundwater depression cone (Figure 2b), Layers 1 and 2, with depths ranging from 13 to 60 m, and 80 to 150 m, respectively, were selected as the primary focus of this study.

Source terms included lateral recharge, precipitation infiltration, and irrigation return flow. Sink terms included lateral discharge, groundwater extraction, and actual evapotranspiration. However, the groundwater table in this region typically exceeds 4 m in depth, which surpasses the maximum evaporation depth for unconfined aquifers. When the groundwater table exceeds this maximum depth, the connection between groundwater and evapotranspiration weakens or disappears (Condon and Maxwell, 2019). Consequently, actual evapotranspiration was set to zero in the sink terms. Detailed calculations of the source and sink terms are provided in Supporting Information Text S3. To assess the impact of the omission of evapotranspiration and the flow boundary condition, a sensitivity analysis was conducted. The results of this analysis are presented in Supporting Information Text S4.

The groundwater level on May 31, 2023 was set as the initial hydraulic head, with daily stress periods spanning June 1, 2023 to September 30, 2023 (122 simulation days). To evaluate MAR effectiveness, this study established 20 recharge wells along a cross-section of the Zhi River (see Figure 5a). Six recharge intensity gradients (50–300 $m^3\ d^{-1}$ with increments of 50 $m^3\ d^{-1}$) were implemented to quantify the effects of MAR using floodwater.

3. Results

This section presents the outcomes derived from the integrated multi-scenario framework coupling deep learning with multi-objective optimization and the three-dimensional groundwater numerical model. We assessed the performance of the encoder-decoder LSTM model in predicting groundwater levels and the groundwater numerical model in predicting groundwater dynamics. Furthermore, we characterize the Pareto frontier distributions, identify the best and worst solutions for each objective function across the different scenarios and quantify the effects of MAR under varying floodwater rates.

3.1 Ecological Flow and Maximum Discharge

As critical constraints, the determination of ecological flow and maximum discharge directly influenced the optimization outcomes. The Tennant method was employed to calculate historical monthly average river flow, which served as the baseline for ecological flow assessment due to its wide applicability under limited flow data conditions. Long-term records showed recurrent zero-discharge episodes during the flood season, which depressed the multi-year monthly means. As an illustration, during the 2023 flood season there were 57 consecutive zero-flow days from June 1 to July 27 (Figure S1 in Supporting Information). Accordingly, to maintain suitable aquatic habitats, ecological flow thresholds were set at 60% of monthly averages during flood seasons and 30% in non-flood seasons (Table 1), since flows within 60–100% of the natural regime sustain good habitat conditions, while 30–60% meet basic ecological requirements (Tennant, 1976). Implementing these ecological flow constraints in 2023 eliminated downstream river drying during the flood season, reducing zero-flow days from 57 to 0, which effectively restored continuous flow connectivity and improved the stability of downstream aquatic habitats.

Table 1. Results of multi-year average ecological river flow calculations (1961–2023).

Month	Average River Flow ($m^3\ s^{-1}$)	Ecological River Flow ($m^3\ s^{-1}$)

1	0.113	0.034
2	0.105	0.032
3	0.574	0.172
4	0.871	0.261
5	1.075	0.322
6	0.833	0.500
7	1.551	0.930
8	2.339	1.404
9	0.584	0.350
10	0.723	0.217
11	0.474	0.142
12	0.294	0.088

Historical extreme discharge events were analyzed through empirical frequency analysis of annual maximum discharge records. Documented events included a 200-year return period flood (2,448 $m^3\ s^{-1}$) in 1963 and a 100-year return period flood (1,016 $m^3\ s^{-1}$) in 1996. The unified empirical frequency analysis, combined with Pearson Type III distribution curve fitting, demonstrated excellent model performance (R^2=0.96), confirming the ability of the distribution to statistically characterize discharge extremes (Figure S2 in Supporting Information). When adopting a 2% exceedance probability standard (i.e., a 50-year return period), the maximum discharge for flood safety was determined to be 734 $m^3\ s^{-1}$, which was selected to ensure adequate flood protection for downstream urban areas.

These two constraints, including minimum ecological flow and maximum discharge threshold, jointly defined the feasible solution space of the optimization process. The minimum ecological flow limits excessive water retention in the reservoir, thereby ensuring continuous downstream flow connectivity even under low-inflow conditions. In contrast, the maximum discharge threshold limits excessive flood releases, thereby preventing downstream flood hazards. Consequently, these constraints confined the optimization results within a reasonable range, ensuring that downstream ecological requirements were satisfied while maintaining sufficient flood-control capacity.

3.2 Groundwater Level Prediction Effect

To optimize the predictive accuracy of the encoder-decoder LSTM model, we evaluated its performance by tuning the input sequence length (m), which governs the temporal dependency window through which the model captures hydrological memory. In this context, m represents the time horizon over which antecedent groundwater levels, precipitation, potential evaporation, and reservoir discharge collectively influence groundwater dynamics. Short sequences may fail to capture delayed hydrological feedback, whereas long sequences may introduce redundant temporal information. Comparative performance metrics across different m varying from 1-15 days are illustrated in Figures 6a-o. While maintaining superior training performance ($R^2 > 0.93$, $MSE < 0.2$) for all m, testing accuracy showed notable variability. m of 5–11 days yielded robust testing set performance ($R^2 > 0.85$, $MSE < 0.02$), indicating strong correlations between hydrological inputs (including precipitation, evaporation, and discharge) and groundwater levels. The model performed optimally on the testing set at $m = 6$ days ($R^2 = 0.93$, $MSE = 0.008$), followed closely by $m = 9$ days ($R^2 = 0.92$, $MSE = 0.010$). This superior performance corresponds to the characteristic lag between precipitation, evaporation, reservoir releases, and groundwater level responses, indicating that the model effectively captured short-term surface–subsurface interactions. Accordingly, these two configurations were selected for integration into the coupling framework in subsequent studies: $m = 6$ for the primary groundwater level predictions in the coupling framework due to its superior performance, and m = 9 for subsequent sensitivity analyses to assess the robustness of optimization outcomes.

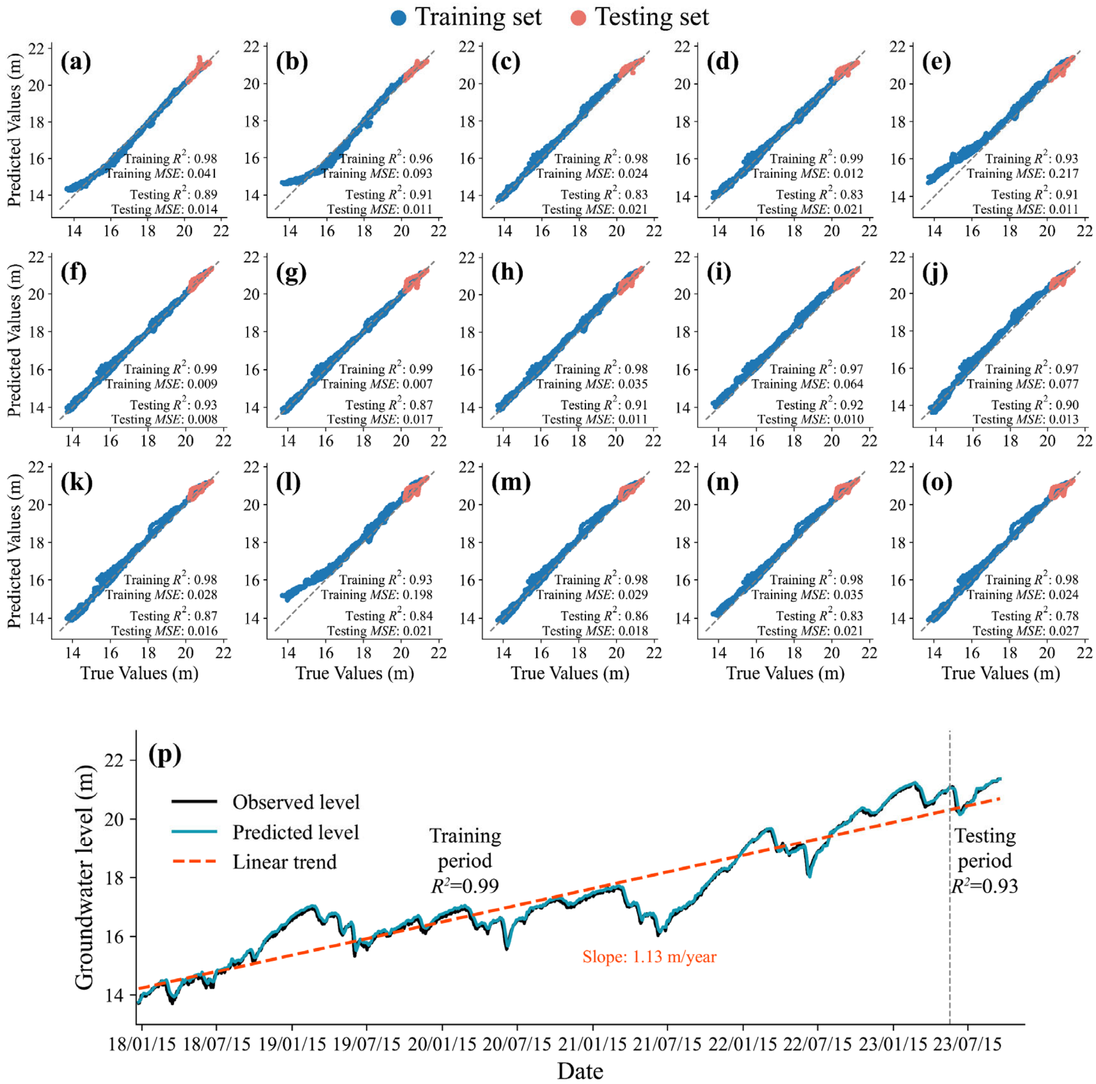

Figure 6. Results of the groundwater level prediction of the encoder-decoder LSTM Model: (a)-(o) model performance on the training and testing sets for input sequence length of 1-15 days; (p) fitting effect of groundwater dynamics with an input sequence length of 6 days, where the black solid line, blue solid line, and red dashed line represents the observed, predicted groundwater level, and the trend of groundwater level changes during the prediction period.

The encoder-decoder LSTM model performed effectively in predicting groundwater dynamics at an input sequence length of 6 days. As demonstrated in Figure 6p, the model achieved high predictive performance, with training period accuracy (R^2=0.99) and testing period generalization capacity (R^2=0.93).

The predicted groundwater level series closely matched the observed values over time throughout the monitoring period, even during extreme water level fluctuations. Additionally, groundwater levels exhibited an upward trend throughout the prediction period, with a long-term trend (see the fitted line in Figure 6p) indicating an average annual groundwater recovery rate of 1.13 m, which resulted from the implementation of effective groundwater management and control measures in the study area. Consequently, this m = 6 configuration was selected for groundwater prediction in subsequent multi-objective optimization.

3.3 Pareto Frontier Distribution

Based on the previously determined input length of m = 6 days, the encoder-decoder LSTM model was incorporated into the coupled deep learning and multi-objective optimization framework. Through iterative optimization computations, this study generated the two-dimensional projections of the original three-objective Pareto front for the Lincheng Reservoir system under varying FLWL scenarios (Figure 7). The depicted box plots (the diagonal graphs in Figure 7) quantitatively characterize the distributional properties of each objective, while the scatter plots (the off-diagonal graphs in Figure 7) illustrate the inverse and positive relationships among competing objectives. Additionally, the Spearman’s rank correlation coefficient (ρ) reflected the strength of these relationships. Negative correlations ($\rho < 0$) denote inverse relationships, where improvements in one objective (e.g., reducing reservoir flood risk) come at the expense of another (e.g., increasing reservoir water scarcity), necessitating compromises in decision-making to balance competing priorities. In contrast, positive correlations ($\rho > 0$) indicate advancements in one objective simultaneously support or enhance the other, enabling optimization without inherent conflicts. Figure 7 shows that there exists a detectable inverse relationship between the reservoir flood risk and reservoir water scarcity objectives across all scenarios. The negative ρ values among these two factors (all below -0.99) in all scenarios indicated that it was challenging to reduce both reservoir flood risk and water scarcity simultaneously through optimized scheduling. Reservoir water scarcity objectives exhibited positive relationships with groundwater recovery targets ($\rho > 0.60$ in all scenarios), while reservoir flood risk objectives demonstrated inverse characteristics with groundwater recovery ($\rho < -0.59$ in all scenarios). When reservoir discharge decreased, water storage in the reservoir increased, more inflow was retained within the reservoir, and consequently elevating reservoir flood risk during the flood season while reducing reservoir water scarcity risk at the end of the flood season. Meanwhile, the reduced downstream release decreased the available infiltration, leading to weaker groundwater recovery effects. Therefore, reservoir flood risk exhibited inverse relationships with both reservoir water scarcity and downstream groundwater recovery, whereas reservoir water scarcity and groundwater recovery showed a positive relationship. This outcome is consistent with the fundamental principles of water balance in the hydrological cycle.

The groundwater recovery targets calculated in all scenarios were relatively small, with values on the order of 10^{-5}. These values are dimensionless, as they were calculated as the ratio of groundwater recovery to the original groundwater level, representing relative rather than absolute changes. This confirmed that relying solely on discharge flow regulation for groundwater recovery was substantially limited and further indicated that, within the imposed operational constraints, the variations in reservoir discharge induce only minor changes in downstream river flow compared with other groundwater source and sink terms.

With the transition from Scenario *a* to Scenario *c*, ρ between reservoir water scarcity and groundwater recovery decreased from 0.872 to 0.612, while that between reservoir flood risk and groundwater recovery was also weakened from –0.872 to –0.598. This weakening of both positive and negative correlations arises because raising the FLWL allowed more water to be stored in the reservoir, increasing its storage capacity. As a result, both reservoir flood risk and reservoir water scarcity risk declined, whereas groundwater recovery diminished because reduced downstream releases recharge led to less infiltration. This adjustment increased the influence of storage capacity on both flood risk and reservoir water scarcity, while groundwater recovery remained primarily controlled by reservoir discharge. Consequently, elevating the FLWL across different scenarios reduces the direct competition between flood control and reservoir water storage, enabling simultaneous enhancements in flood control safety and water storage benefits. These shifts altered the mechanisms linking the objectives, thereby attenuating the strength of their inverse or positive relationships.

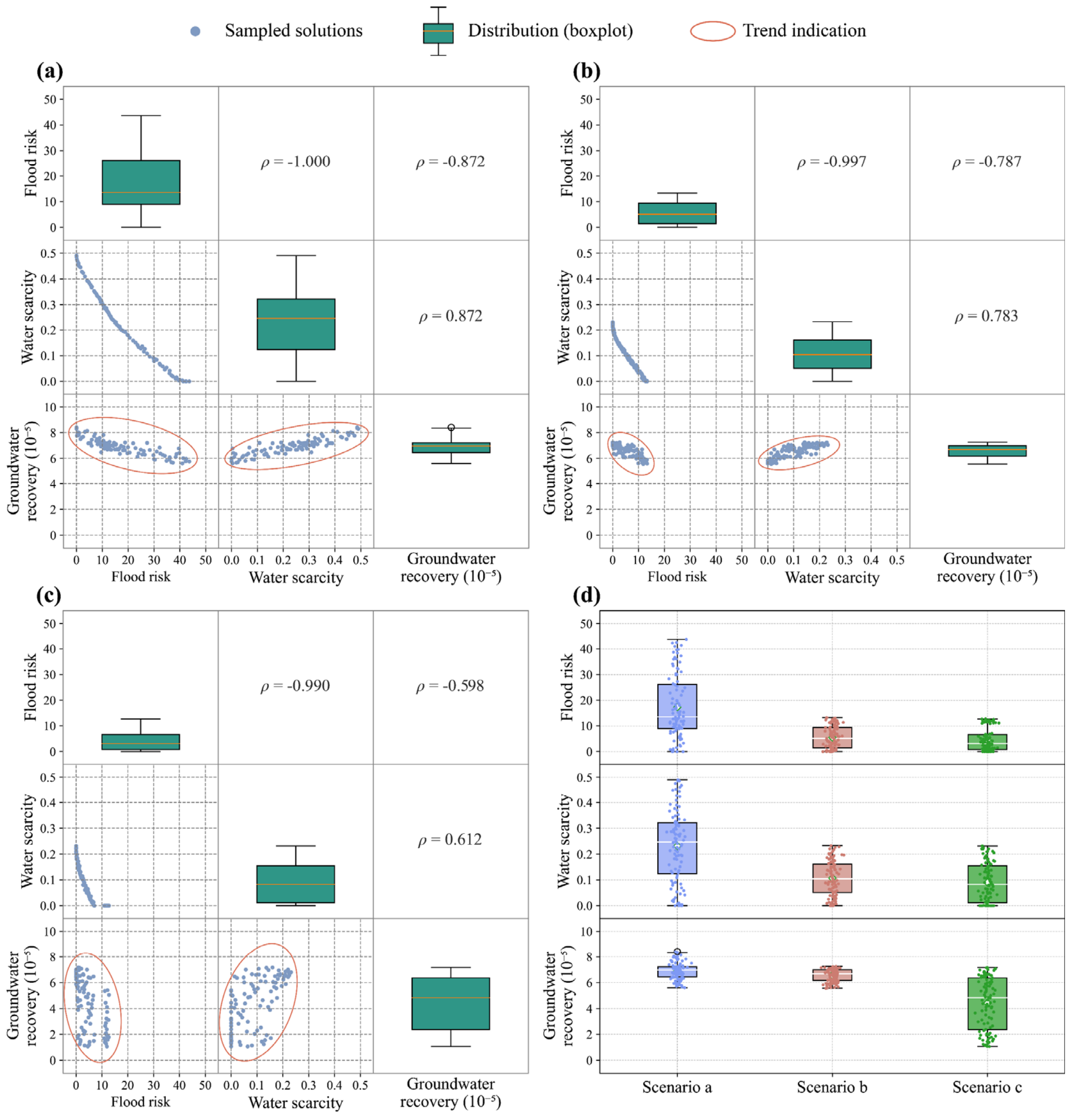

Figure 7. Two-dimensional matrix diagram of the Pareto front for an input sequence length of 6 days for (a) Scenario *a*, (b) Scenario *b*, and (c) Scenario *c*, illustrating the relationships among the three optimization objectives: flood risk, water scarcity, and groundwater recovery. Blue scatter points represent the optimized solutions, red ellipses indicate the overall inverse or positive trends between objectives, and ρ quantifies the strength and direction of these relationships. Green boxplots along the diagonal show the distribution of each objective within its respective scenario. (d) compares the distributions of the three objectives across the three FLWL scenarios, revealing the sensitivity of the optimization outcomes to different reservoir water-level constraints.

Adjustments to FLWL induced substantial changes in the Pareto front objective values (Figure 7d). Increasing FLWL (Scenarios *a*-*c*) reduced flood risks by 84.9% and water scarcity risks by 61.9%, confirming that an increase in FLWL within safe operational thresholds enables the dual-objective optimization of flood control and water storage. This improvement arises because a higher FLWL increases the storage capacity of the reservoir, thereby lowering the probability of FLWL exceedance while allowing more water to be retained for subsequent use, which consequently reduces water scarcity losses at the end of the flood season. However, the accompanying decrease in downstream discharge reduces river-aquifer interactions, thereby weakening groundwater recovery by 22.2%. Groundwater recovery targets remained positive (>0) across all scenarios, demonstrating that maintaining regulated ecological flow thresholds effectively mitigates groundwater level deterioration even under diminished total discharge conditions. However, groundwater recovery remained limited across all scenarios. This suggested that while maintaining ecological flow, which facilitated groundwater recovery, additional effective measures were still required to achieve rapid groundwater recovery.

3.4 Best and Worst Solution for Each Objective

As demonstrated in previous sections, distinct positive or inverse relationships existed between different objectives. In the next step, the best and worst solutions for each objective were then analyzed to assist decision-makers in selecting management strategies based on different priorities. Figure 8 illustrates the solutions for each objective across scenarios. The results revealed substantially larger discharge volumes during peak flood periods (July 30 to August 1) compared to other periods under all scenario-solution combinations.

The best solution for flood control (the first row graphs in Figure 8) kept the reservoir levels below the corresponding FLWL throughout all operational periods (F_1 in Equation 3 equals 0). Given the pronounced inverse relationships between flood risk and reservoir water scarcity objectives, this solution also represented the worst solution for water storage in Scenarios a and b (Figures 8a4 and 8b4) or closely approximates it in Scenario c (Figure 8c4), thereby highlighting the direct conflict between minimizing reservoir flood risk throughout the flood season and ensuring adequate storage at the end of the flood season. The stringent implementation of FLWL operation strategies resulted in waste of floodwater resources. The floodwater utilization rate (i.e., utilized flood volume/total flood volume) stayed below 25% across all scenarios, even dropping below 5% in Scenario *a*. This outcome arose because higher outflows led to lower reservoir levels, preventing full utilization of storage capacity. As a result, floodwater was primarily released rather than being retained for future use, resulting in low floodwater utilization efficiency. Consequently, reservoir water levels at the end of the flood season became critically low, making rapid restoration to normal storage level operationally challenging.

The best solution for water storage (the third row graphs in Figure 8) improved floodwater utilization, with resource utilization rates approaching 40% across all scenarios. This operational strategy raised reservoir levels to normal storage capacity by the end of the flood season (F_2 = 0). However, this solution also represented the worst solution for flood control (the second row graphs in Figure 8). This implementation resulted in reservoir level exceedances above FLWL for 62 days (Scenario *a*), 51 days (Scenario *b*), and 26 days (Scenario *c*), respectively. This trend was driven by the increase in FLWL, which expanded the allowable storage space, thereby reducing the frequency of exceedances under the same storage strategy.

The best solution for groundwater recovery (the fifth row graphs in Figure 8) within the optimization framework showed operational patterns similar to the best solution for flood control (the first row graphs in Figure 8), with reservoir levels remaining below the FLWL. While this strategy maximized the groundwater recovery objective relative to other feasible operations, its absolute efficacy remained limited, since a considerable portion of floodwater releases could not be effectively converted into subsurface storage. This limitation arose because the duration of flood peaks was short, and the limited short-term infiltration restricted substantial groundwater recharge during the flood season. This also highlights the limitation of relying solely on reservoir release regulation for groundwater recovery.

The worst solution for groundwater recovery (the sixth row graphs in Figure 8) was characterized by minimal reservoir discharge, which substantially reduced groundwater recharge and produced the lowest recovery effects. Because of the reduced outflow, the reservoir retained higher water levels by the end of the flood season, generally remaining close to the normal storage level.

While the best and worst solutions for each objective cannot achieve optimization of all objectives simultaneously, a moderate elevation of FLWL facilitated simultaneous reduction of both flood and water scarcity risks. However, as indicated by the limited groundwater recovery across scenarios, additional measures such as managed aquifer recharge (MAR) are necessary to enhance groundwater recovery. Accordingly, the following section evaluates groundwater numerical simulations and quantifies the impacts of MAR under varying recharge rates.

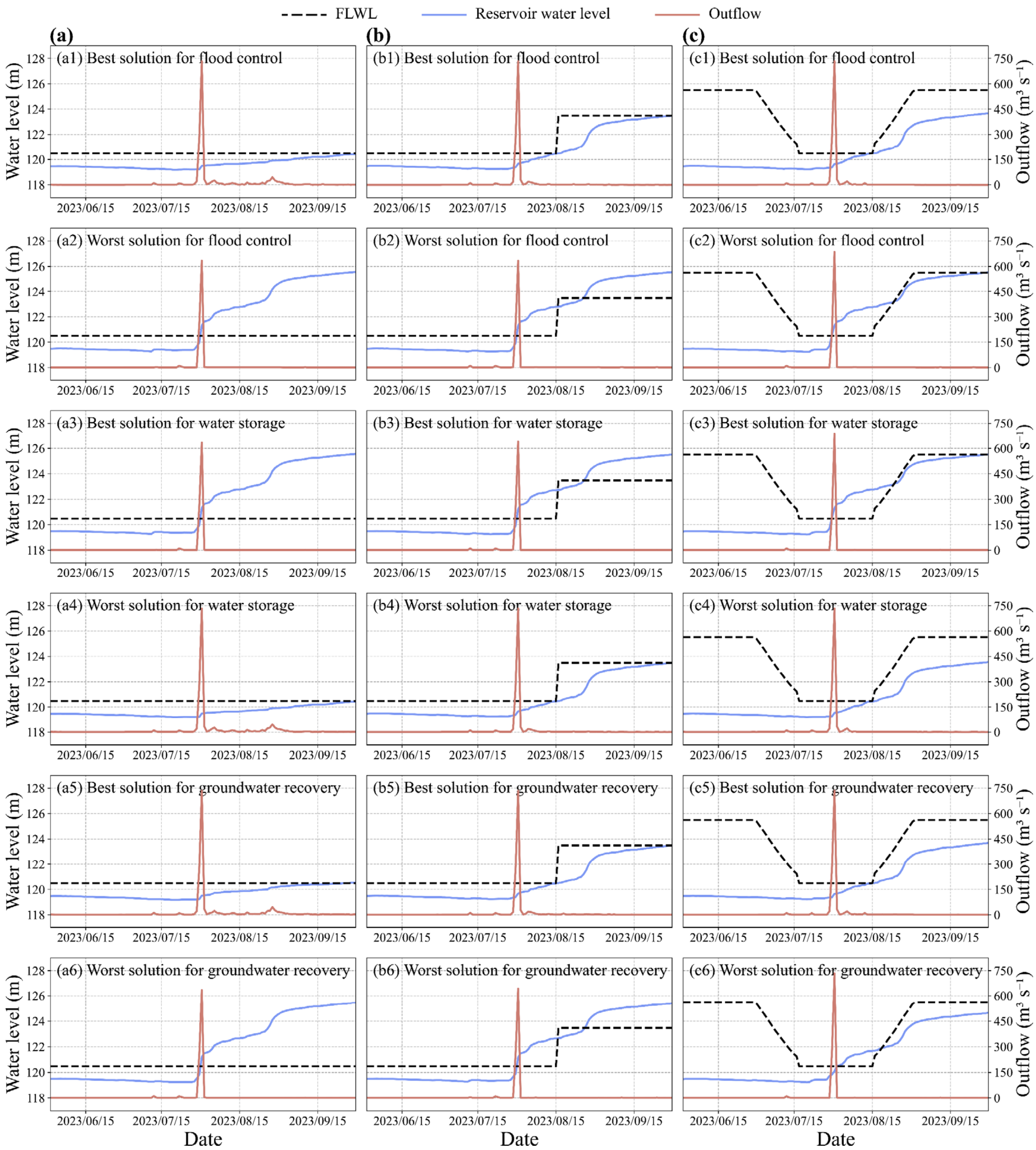

Figure 8. Best and worst solution for each objective under Scenarios *a*, *b*, and *c*. The first and second row graphs show the best and worst solutions for flood control, the third and fourth row graphs for water storage, and the fifth and sixth row graphs for groundwater recovery. The best solution for flood control maintains reservoir levels below corresponding FLWL throughout all operational periods, while the best solution for water storage achieves normal storage level by the end of flood season.

3.5 Effectiveness of Groundwater Numerical Simulation

To further investigate the effective floodwater utilization strategies, the proposed MAR scheme was tested, whereby accurate simulation of groundwater dynamics served as the essential basis for evaluating the feasibility of this strategy. To evaluate MAR feasibility, the MODFLOW model was employed to simulate groundwater dynamics. A comparative analysis of simulated and observed groundwater levels at six monitoring wells (i.e., Zhongzhang, Xiyin, Tunli, Beicun, Maoshanying, and Longyao) is presented in Figure 9.

Overall, the simulated results demonstrated strong agreement with observed trends, indicating that the model effectively captured groundwater level dynamics. Most monitoring wells exhibited satisfactory calibration performance, with R^2 ranging from 0.82 to 0.96 and *MSE* between 0.0006 and 0.016 m, confirming the robustness of the simulation accuracy. These results validated the applicability of MODFLOW for providing reliable support for the quantitative assessment of managed aquifer recharge effectiveness.

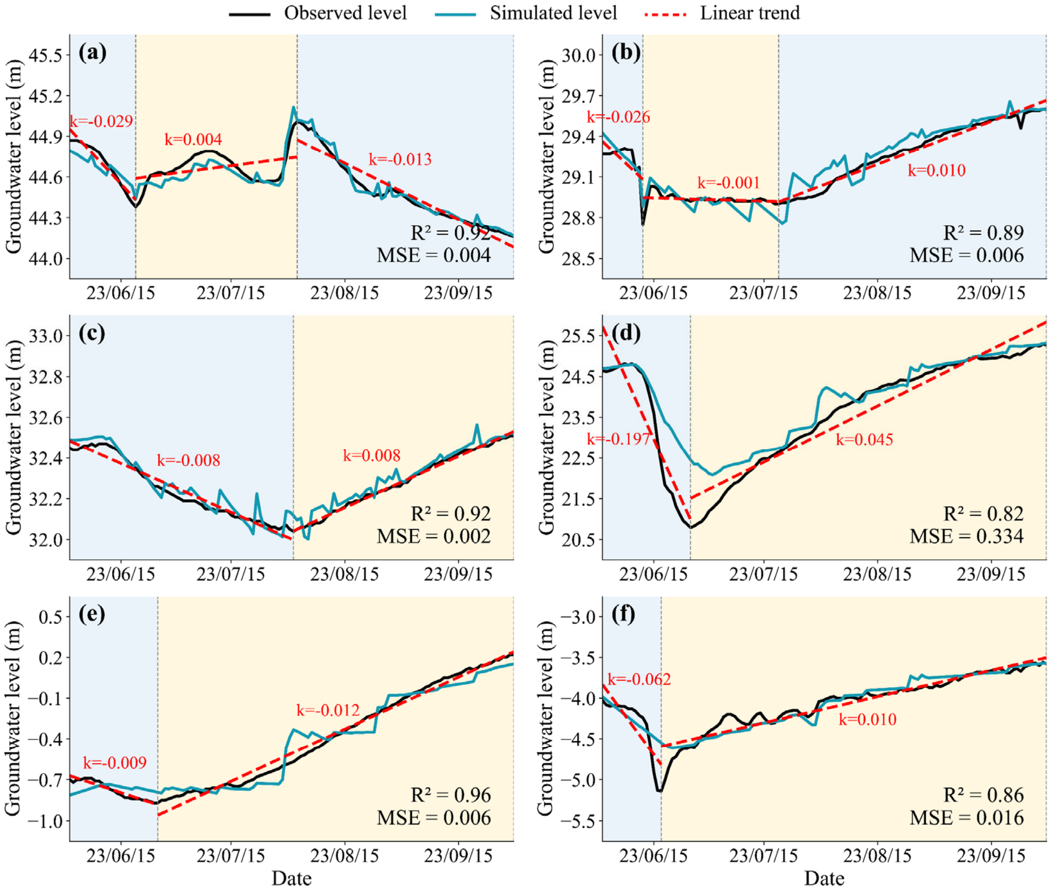

Figure 9. Comparison of measured and simulated groundwater levels at different monitoring wells. (a) Zhongzhang, (b) Beicun, (c) Xiyin, (d) Tunli, (e) Maoshanying, and (f) Longyao, with the black solid line representing the measured level, the blue solid line the simulated level, and the red dashed line the long-term linear trend. Different background colors distinguish various trend stages during the simulation period.

During the simulation period, the groundwater levels of six monitoring wells exhibited distinct stage trends. For most wells (excluding Zhongzhang and Beicun in Figures 9a-b), the levels exhibited a decline in groundwater levels before recovering. In contrast, the measured and simulated groundwater level at Zhongzhang well exhibited a declining trend, followed by a slow increase, and a followed decline. The level at Beicun (Figure 9b) also exhibited a trend of decline, whereby the second phase was characterized by stabilization, and a followed increase in groundwater levels. The initial decline in groundwater levels across nearly all wells can be associated with high groundwater extraction used for spring irrigation, while the subsequent increases were driven by substantial precipitation during the flood season. These deviations can be attributed to localized groundwater extraction, which induced additional fluctuations in the groundwater levels at these two wells.

3.6 Investigation on Efficient Utilization of Flood Resources

Leveraging the validated MODFLOW model, we quantified the spatial and quantitative effects of MAR using floodwater resources under varying recharge rates, as illustrated in Figure 10. Due to varying hydrogeological conditions in the area, the groundwater recovery levels exhibited spatial heterogeneity. As can be seen, groundwater recovery primarily occurred around the Zhi River, with more pronounced recovery observed in the western regions compared to the eastern regions. This difference might arise from the smaller specific yield in the west, where limited aquifer storage capacity causes the same recharge volume to produce a high rise in groundwater levels. By assuming recharge intensities from the 20 recharge wells ranging from 50 to 300 m^3 d^{-1}, the proportion of the effective groundwater recovery area also varied and increased from 9.3 to 17.6%. Simultaneously, the average recovery in the effective recovery areas increased from 0.01 m to 0.09 m. The maximum groundwater recovery exhibited a distinct three-phase nonlinear pattern in response to varying recharge rates. In phase I, with recharge rates of 50 - 100 m^3 d^{-1}, the maximum recovery level surged from 0.06 m to 0.36 m, as the aquifer’s recharge potential was high at this stage. In phase II, with recharge rates of 100-200 m^3 d^{-1}, it stabilized at 0.36 m, suggesting a diminishing response as additional recharge no longer produced proportional increases in groundwater levels. In phase III, with the highest recharge rates of 200-300 m^3 d^{-1}, the recovery gradually increased from 0.36 m to 0.46 m, since enhanced recharge expanded the groundwater recovery zone, leading to a further rise in water levels but with a smaller magnitude than that in phase I. As shown in Figure 10g, the recovery rate significantly improved between recharge rates of 50 and 100 m^3 d^{-1} ($p < 0.05$), indicating a marked response within this recharge rates range. This pattern demonstrates that increasing recharge intensity enhances groundwater recovery levels, but the effect might be weakened as the aquifer approaches its limits.

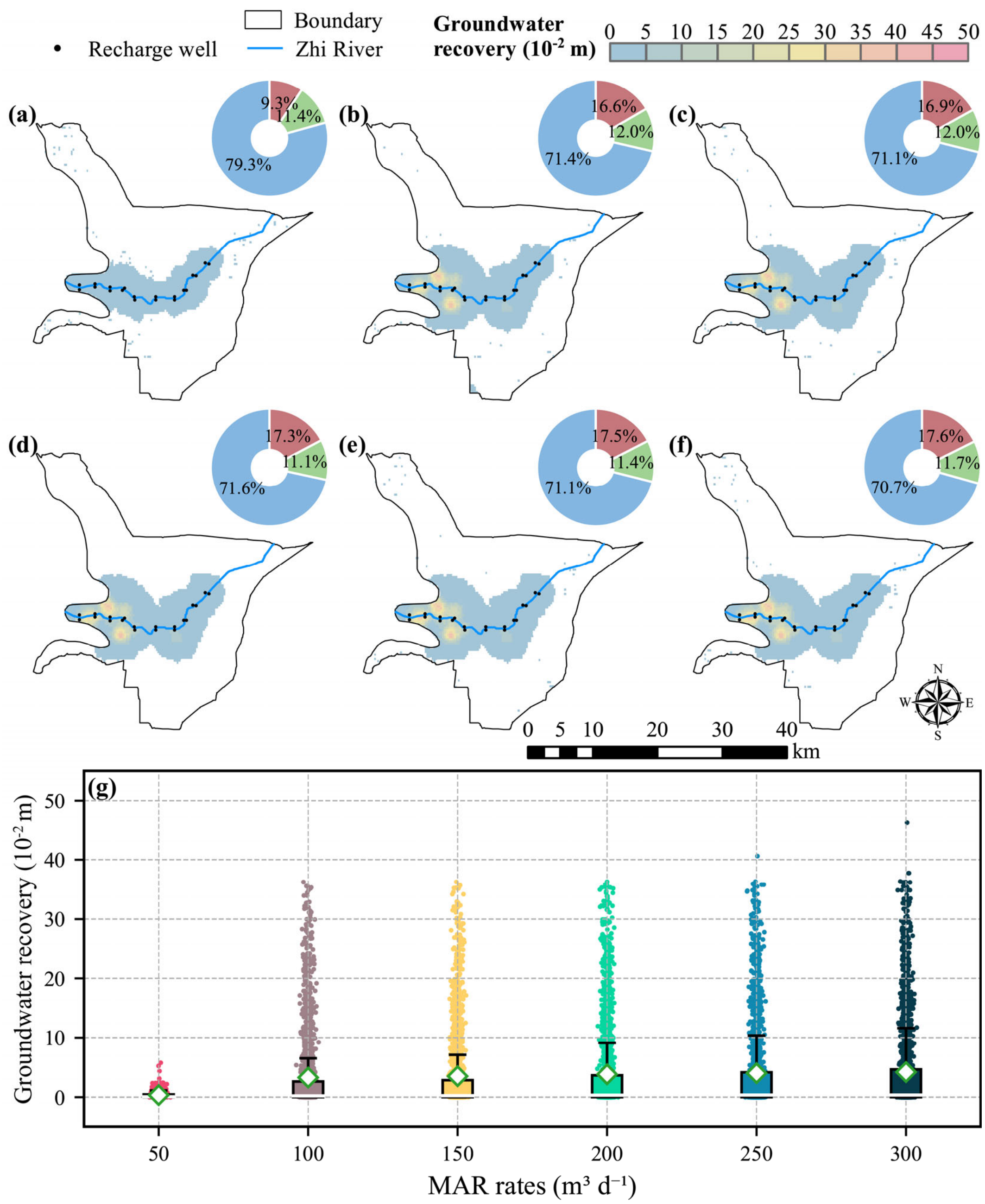

Figure 10. Spatial distribution of groundwater recovery under varying recharge rates in the 20 wells. (a) 50, (b) 100, (c) 150, (d) 200, (e) 250, and (f) 300 m^3 d^{-1}. Blue lines represent river, and black dots denote recharge wells. The inset pie chart illustrated the proportion of areas with different recovery levels: blue indicated unrecovered areas (recovery = 0 m), green showed inefficient recovery areas (0 < recovery < 0.01 m), and red denoted effective recovery areas (recovery > 0.01 m). (g) the distributions of recovery values (> 0 m) across different recharge rates, presented as boxplots and scatter points, where mean values are denoted by diamonds.

This pattern is consistent with the findings of Samanta et al. (2020) on recharge volume-dependent infiltration rate thresholds. Therefore, the effective implementation of MAR should consider the spatial heterogeneity of aquifer permeability, optimize recharge rates, and consider land use constraints (Owuor et al., 2016) to avoid inefficient percolation zones, while balancing recovery efficacy with engineering costs.

4. Discussion

While the aforementioned results demonstrate the effectiveness of the proposed floodwater utilization framework, including the performance evaluation of the groundwater numerical model, and the quantification of MAR effects using floodwater resources, several key aspects merit further examination to contextualize these findings and inform future applications. Accordingly, this discussion first examines the sensitivity of optimization outcomes to variations in the encoder-decoder LSTM input sequence length, MAR recharge rates and decision variable, before addressing the limitations and potential risks.

4.1 Impact of Input Sequence Length of the Groundwater Level Prediction Model on Optimization Results

The developed deep learning and multi-objective optimization framework effectively quantified competing objectives. However, as one of the key hyperparameters, which are user-defined settings that govern model architecture and training, the input sequence length m has a significant impact on the predictive performance of LSTM models (Gauch et al., 2021; Hosseini et al., 2024). While the configuration with m = 6 days was selected as suitable based on comprehensive training and testing performance metrics, the model with m = 9 days showed comparable robustness (Figure 6). To examine the impact of this hyperparameter on optimization results, the 9-day model was integrated into the multi-objective framework, generating alternative Pareto front solutions (Figure 11).

The results indicated that adjustments to m affect the objective function values across all objectives. Flood risks and water scarcity showed no significant differences ($p > 0.05$) between the two configurations analyzed. Groundwater recovery objectives exhibited significant differences ($p < 0.05$) but maintained consistently positive objective function values. This demonstrated that the continuous maintenance of river flow was critical for effective groundwater recovery.

Notably, changes of input sequence length (from 6 to 9 days) did not alter inter-objective inverse or positive effects. Flood risk maintained inverse relationships with reservoir water scarcity and groundwater recovery, while water scarcity and groundwater recovery retained a positive relationship. Similarly, this change of m also did not affect the response of objectives across the different scenarios. When FLWL was elevated, flood risks and reservoir water scarcity losses significantly decreased ($p < 0.05$) when moving from $m = 6$ to 9 days configuration. At the same time, the inverse or positive relationships between objectives became weakened (the absolute value of ρ decreased). This indicated that increasing FLWL could reduce competition between multi-objectives optimization and promote system balance. Changes in m did not alter the relationships between objectives. However, its limitations still persist, as variations in sequence length may impact model performance under different hydrological conditions or when applied to new scenarios.

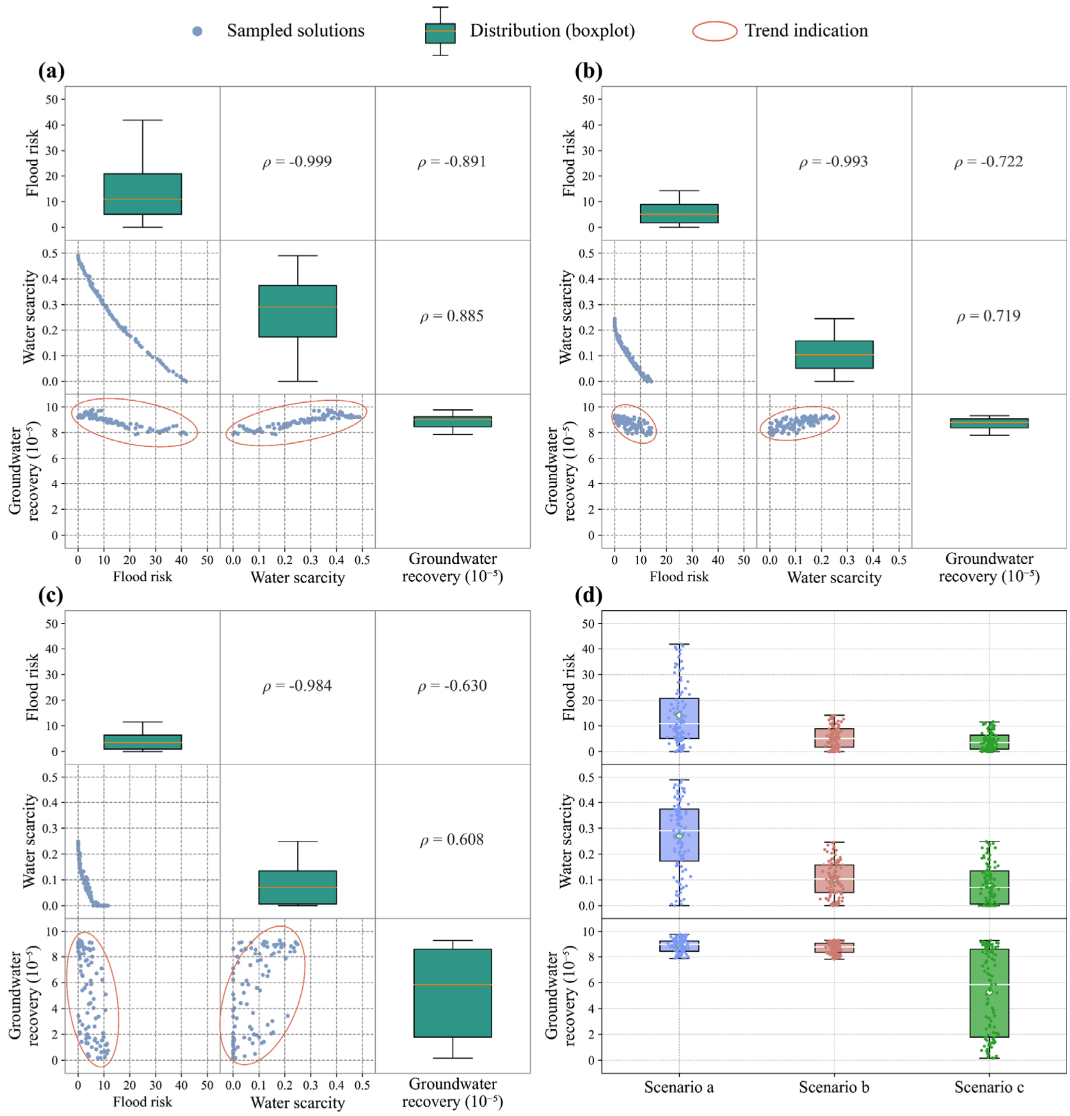

Figure 11. Two-dimensional matrix diagram of Pareto front competition when input sequence length was set to 9 days under (a) Scenario *a*, (b) Scenario *b*, and (c) Scenario *c*, illustrating the relationships among the three optimization objectives: flood risk, water scarcity, and groundwater recovery. The blue scatters show relationships between objectives, the red ellipses indicate the overall trend of the scatter points, the green box show the distribution of each objective within its respective scenario., and ρ reflects the strength of positive or inverse relationships. (d) compares the distributions of the three objectives across the three FLWL scenarios, revealing the sensitivity of the optimization outcomes to different reservoir water-level constraints.

4.2 Impact of Managed Aquifer Recharge on Optimization Results

Based on the quantified benefits of MAR on groundwater recovery as demonstrated in previous sections, this section explores its broader implications for the multi-objective optimization framework, particularly during the implementation of MAR, how the minimum discharge within the multi-objective optimization framework satisfy both ecological and recharge flow requirements. Consequently, Equation 6 was accordingly modified as follows:

$$Q_t \geq Q_t^{eco} + Q_{MAR} \tag{11}$$

where Q_{MAR} represents the flow required for different recharge rates [L^3T^{-1}], while other variables remain consistent with Equation 6. This modification ensures that the minimum release constraint not only maintains downstream ecological flow but also guarantees sufficient water availability for MAR implementation.

Following this adjustment, the relationship between flood risk and water scarcity was examined, with results presented in Figure 12. Despite the adjustment in constraints, the inverse relationships between flood risk and water scarcity persisted. In the multi-objective optimization process, MAR was represented as an increased minimum discharge constraint (Equation 11). Under this constraint, the simulations showed that MAR led to lower average flood risk but higher average reservoir water scarcity. This outcome is evident in all the inset box plots of Figure 12, where applying MAR shifts the mean values (cross symbols) downward for flood risk (brown columns, left without MAR to right with MAR) and upward for water scarcity (orange columns). This change might result from the increase in the minimum discharge constraint under MAR, which needs more water to be released downstream, thereby reducing flood risk while simultaneously increasing reservoir water scarcity losses at the end of the flood season. Statistical tests, as indicated by the p-values shown in each inset box plot, further confirmed that these differences were significant ($p < 0.05$) only at the highest recharge rate of 300 m^3 d^{-1} (Figure 12f), while no significant differences ($p > 0.05$) were observed at lower recharge rates (Figures 12a–e). This is because at lower recharge rates, the changes in the minimum discharge constraint were relatively small, resulting in limited impacts on the optimization outcomes.

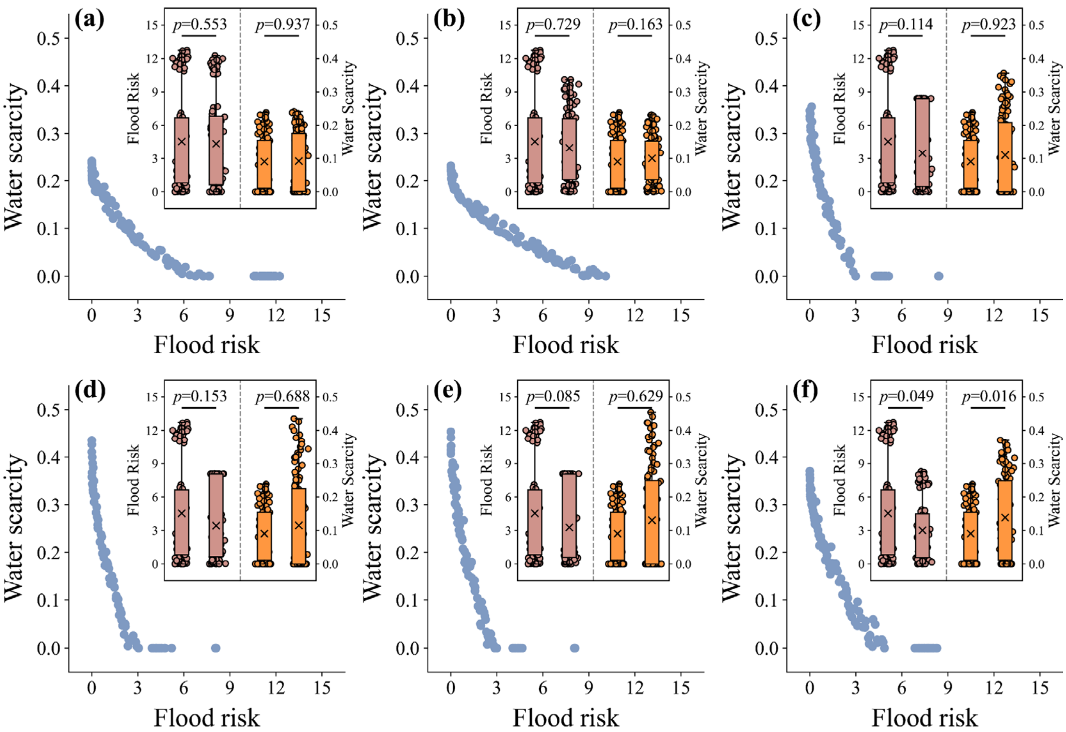

Figure 12. The relationship between flood risk and water scarcity under different managed aquifer recharge (MAR) rates. (a)-(f) show the results under recharge rates of 50, 100, 150, 200, 250, and 300 m^3 d^{-1}, respectively. Inset box plots compare flood risk (brown column) and water scarcity (orange column) without (left bar) and with (right bar) recharge measures. Cross (×) represents average value. Statistical tests *p*-values are also indicated in the inset box.

Figure 12. The relationship between flood risk and water scarcity under different managed aquifer recharge (MAR) rates. (a)-(f) show the results under recharge rates of 50, 100, 150, 200, 250, and 300 m^3 d^{-1}, respectively. Inset box plots compare flood risk (brown column) and water scarcity (orange column) without (left bar) and with (right bar) recharge measures. Cross (×) represents average value. Statistical tests *p*-values

are also indicated in the inset box. Similar findings have been reported in previous studies. Schäffer et al. (2022) emphasized that maximum discharge constraints significantly affect the marginal water values (i.e., the opportunity cost of storing water for future power generation) as well as the operational strategies of hydropower systems. Helseth et al. (2022) demonstrated that environmental constraints could complicate scheduling problems by introducing state dependencies and non-convexities. Increasing downstream water demand could improve flood utilization efficiency as shown by Wang et al. (2022). These studies highlighted that variations in constraints influence optimization outcomes. Thus, defining and incorporating constraints, such as those introduced by MAR in this study, is crucial for achieving robust and balanced reservoir optimization outcomes, ensuring that floodwater utilization aligns with multiple objectives including ecological sustainability and groundwater recovery.

4.3 Impact of Decision Variable on Optimization Results

To assess the robustness of the optimization scheme, we evaluated the sensitivity of the results to the choice of decision variable. In Section 2.3.3, we initially used the outflow-to-inflow ratio as the decision variable (Decision Variable 1). As Yang et al. (2017) demonstrated, the efficacy of decision variables can differ significantly across scenarios, especially under uncertain or extreme events, potentially leading to suboptimal outcomes. Therefore, we introduced an alternative decision variable, i.e., the outflow relative to the previous day's reservoir storage (Decision Variable 2). Subsequently, we applied this new decision variable to multi-objective optimization simulations under three FLWL scenarios, which were described in Section 2.3.1. The comparative results are presented in Table 2.

All objective values exhibited significant differences ($p < 0.05$) between the two decision variables across the three FLWL scenarios. Notably, minimum flood risk and reservoir water scarcity no longer reached zero in any scenario under Decision Variable 2. Despite these quantitative differences, the variation trends of the objectives across scenarios remained consistent with those obtained under Decision Variable 1. Specifically, as the FLWL increased (from Scenario *a* to *c*), the mean values of all objectives decreased. Moreover, the inverse and positive relationships among flood risk, reservoir water scarcity, and groundwater recovery (see Supporting Information Figure S4) followed the same patterns described in Section 3.3. This indicates that while the choice of decision variable can significantly influence the absolute value of the objective functions, it does not alter the intrinsic interactions among the objectives.

Table 2. Comparison of optimization objectives under different decision variables. Decision Variable 1 and 2 are the outflow-to-inflow ratio and the outflow relative to the previous day's reservoir storage, respectively.

Objectives	Scenarios	Decision Variable 1		Decision Variable 2		*p*
		Average	Range	Average	Range	
Flood Risk	*a*	17.33	[0, 45.65]	12.63	[4.60, 25.56]	<0.05
	b	5.53	[0, 13.29]	8.56	[4.56, 15.33]	<0.05
	c	4.54	[0, 12.73]	7.85	[4.61, 13.07]	<0.05
Water Scarcity	*a*	0.23	[0, 0.49]	0.36	[0.21, 0.51]	<0.05
	b	0.11	[0, 0.23]	0.28	[0.11, 0.54]	<0.05
	c	0.09	[0, 0.22]	0.23	[0.14, 0.36]	<0.05
Groundwater Recovery (10^{-5})	*a*	6.92	[5.61, 8.42]	9.61	[7.67, 12.16]	<0.05
	b	6.57	[5.56, 7.26]	7.55	[3.75, 10.29]	<0.05
	c	4.42	[1.06, 7.17]	4.42	[2.55, 5.81]	<0.05

4.4 Advantages, Limitations and Potential Risks

The developed deep learning and multi-objective optimization scheme, leveraging an encoder-decoder LSTM architecture, offers advantages in groundwater level prediction and optimization. Deep learning models excel at capturing complex non-linear dependencies from historical data. This is especially advantageous when complete data on source-sink terms are difficult to obtain, as the utilized encoder-decoder LSTM can capture the underlying relationships in the system through data-driven learning (Solgi et al., 2021). Moreover, deep learning models are computationally efficient, enabling them to process large datasets efficiently and integrate seamlessly into optimization schemes. This makes them valuable for large-scale optimization tasks, whereas traditional physics-based models might be more computationally intensive (He et al., 2022; Tripathy and Mishra, 2024).

Although this study advances a robust framework for multi-objective optimization of flood control, water storage, and groundwater recovery by integrating deep learning and 3D groundwater numerical modeling, several limitations constrain its scope and applicability, highlighting avenues for future work. First, a key limitation of using the deep learning model is its limited adaptability to replacing traditional physical models across diverse scenarios. Unlike process-based models governed by physical laws, the deep learning models rely solely on statistical patterns. Consequently, it may struggle to generalize to new, unseen conditions, especially in extreme hydrological events caused by climate change (Acuña et al., 2025). Model performance may degrade when applying to extreme conditions, highlighting the need for caution in using the deep learning model as a substitute for traditional physical models.

Second, the framework's exclusive focus on flood-season operations overlooks critical non-flood season dynamics, particularly the regulation of groundwater extraction, which exacerbates depletion in vulnerable depression cone regions. Under climate change, integrating cross-seasonal strategies, such as augmenting flood-season recharge, while curtailing non-flood extraction through adaptive pumping controls (Balerna et al., 2024; Tang et al., 2024), could yield more sustainable outcomes by balancing annual water budgets and mitigating long-term groundwater stress.

Finally, while MAR emerges as a promising tool for floodwater utilization, it introduces potential environmental risks, including water quality degradation and clogging, which could undermine ecological health if not rigorously managed (Fiori et al., 2025; Guo et al., 2023). To mitigate these issues, infiltration and pulsed injection can be applied (Page et al., 2014; Rodríguez et al., 2018), although these measures increase operational costs and limit economic feasibility. This necessitates expanded analyses, explicitly weighing recharge efficiency against water quality through coupled hydrogeochemical modeling.

Despite these limitations and potential risks, the proposed framework’s broader applicability remains promising, as FU under diverse conditions (Ding et al., 2023; Liu et al., 2015) and groundwater recharge practices (Alam et al., 2020; Zhang et al., 2020) are well-established, supporting the effective integration of flood mitigation and groundwater recovery. Therefore, future work can evolve this framework into a more comprehensive, resilient tool for integrated water resource management applicable beyond the North China Plain, particularly under intensifying climate stress.

5. Conclusions

This study advances integrated water resource management by developing a novel coupled framework that merges deep learning (encoder-decoder LSTM) with multi-objective optimization (NSGA-II) and groundwater numerical modeling (MODFLOW) to optimize floodwater utilization in the Lincheng Reservoir system, North China Plain. The framework targets three key objectives: minimizing flood risk (defined as the cumulative exceedance of reservoir water levels above the flood limited water level (FLWL) during the flood season), reducing reservoir water scarcity (measured as the deviation from normal storage levels at the end of the flood season for reservoir), and maximizing groundwater recovery (quantified as the increase in groundwater levels at the end of the flood season resulting from varied reservoir discharge flows during the flood season). By dynamically adjusting reservoir operations across scenarios while ensuring ecological flows and downstream flood safety, the framework demonstrates a pathway for converting flood hazards into resources for groundwater recovery in vulnerable groundwater depression cone areas. The key conclusions are as follows:

1. The encoder-decoder LSTM model exhibited high predictive accuracy for groundwater levels, with optimal performance at a 6-day input sequence ($R^2 = 0.99$ and 0.93 respectively for training and testing) and robust results at 9 days ($R^2 =$ 0.97 and 0.92). This highlights the reliability of the framework in capturing temporal hydrological dependencies.

2. Across all scenarios, flood risk exhibited inverse relationships with both water scarcity and groundwater recovery. Higher flood risk, driven by retaining more

water in the reservoir, reduced reservoir water scarcity through increased storage but limited groundwater recovery by decreasing discharge volumes, thereby reducing the water available for downstream recharge. Increasing the FLWL weakened these inverse relationships, achieving significant reductions in reservoir flood risk and water scarcity (84.9 and 61.9% respectively), with a moderate decrease (22.2%) in groundwater recovery due to lower discharge volumes.

3. Maintaining ecological flows enabled groundwater recovery even under reduced total discharges, emphasizing that continuous river connectivity, rather than volume alone, drives groundwater recharge. This finding challenges conventional volume-focused strategies, advocating for flow continuity as an effective way for groundwater recovery.

4. The MODFLOW model, with accurate replication of spatiotemporal groundwater variations (R^2 of 0.82–0.96), validated managed aquifer recharge (MAR) as an effective enhancement for groundwater recovery in depression cones. At 300 $m^3\ d^{-1}$ operated on 20 recharge wells during the 2023 flood season, maximum recovery reached 0.46 m, with effective recovery (>0.01 m) in 17.6% of the area. Incorporating MAR modified discharge constraints, resulting in lower flood risks and increased water scarcity, illustrating constraint-driven trade-offs that must be balanced in adaptive management. This quantifies MAR's efficacy but highlights spatial heterogeneity and the need for site-specific optimization to maximize benefits.

5. The proposed framework shows potential for broader application beyond the

North China Plain. By transforming flood hazards into recoverable groundwater resources through integrated reservoir operations and groundwater recovery measures, the framework offers a promising strategy for regions facing flood and groundwater depletion risks, advancing climate-resilient water management.

Acknowledgments

This work was supported by the National Natural Science Foundation of China (grant numbers: 4247022276, 42077168) and the National Key R&D Program of China (grant numbers: 2023YFC3006503, 2024YFC3211600). We are grateful to Lei Li from the Ninth Geological Brigade of Hebei Bureau of Geology and Mineral Resources, as well as Yinguo Ren and Yuanyuan Li from the Hebei Provincial Hydrologic Survey and Research Center, for their invaluable assistance in data collection.

References:

Acuña E., E., Loritz, R., Kratzert, F., Klotz, D., Gauch, M. Álvarez C., M. et al., 2025. Analyzing the generalization capabilities of a hybrid hydrological model for extrapolation to extreme events. Hydrology and Earth System Sciences, 29(5): 1277-1294. DOI: 10.5194/hess-29-1277-2025

Alam, S., Gebremichael, M., Li, R.P., Dozier, J. and Lettenmaier, D.P., 2020. Can Managed Aquifer Recharge Mitigate the Groundwater Overdraft in California's Central Valley? Water Resources Research, 56(8). DOI: 10.1029/2020WR027244

Asher, M.J., Croke, B.F.W., Jakeman, A.J. and Peeters, L.J.M., 2015. A review of surrogate models and their application to groundwater modeling. Water Resources

Research, 51(8): 5957-5973. DOI: 10.1002/2015WR016967

Balerna, J.A., Kramer, A.M., Landry, S.M., Rains, M.C. and Lewis, D.B., 2024. Wetland hydrological change and recovery across three decades of shifting groundwater management. Journal of Hydrology, 644: 132052. DOI: 10.1016/j.jhydrol.2024.132052

Bellu, A., Sanches Fernandes, L.F., Cortes, R.M.V. and Pacheco, F.A.L., 2016. A framework model for the dimensioning and allocation of a detention basin system: The case of a flood-prone mountainous watershed. Journal of Hydrology, 533: 567-580. DOI: 10.1016/j.jhydrol.2015.12.043

Bermúdez, M., Farfán, J.F., Willems, P. and Cea, L., 2021. Assessing the Effects of Climate Change on Compound Flooding in Coastal River Areas. Water Resources Research, 57(10). DOI: 10.1029/2020WR029321

Blöschl, G., Hall, J., Parajka, J., Perdigão, R.A.P., Merz, B., Arheimer, B., et al., 2017. Changing climate shifts timing of European floods. Science, 357(6351): 588-590. DOI: 10.1126/science.aan2506

Condon, L. E. and Maxwell, R. M., 2019. Simulating the sensitivity of evapotranspiration and streamflow to large-scale groundwater depletion. Science Advances, 5(6): eaav4574. DOI: 10.1126/sciadv.aav4574

Condon, L.E., Kollet, S., Bierkens, M.F.P., Fogg, G.E., Maxwell, R.M., Hill, M.C., Fransen, H. H., Verhoef, A., Van Loon, A., Sulis, M. and Abesser, C., 2021. Global groundwater modeling and monitoring: Opportunities and challenges. Water Resources Research, 57(12). DOI: 10.1029/2020WR029500

Chagas, V.B.P., Chaffe, P.L.B. and Blöschl, G., 2022. Climate and land management accelerate the Brazilian water cycle. Nature Communications, 13(5136). DOI: 10.1038/s41467-022-32580-x

Chen, X., Wang, P., Muhammad, T., Xu, Z. and Li, Y., 2020. Subsystem-level groundwater footprint assessment in North China Plain – The world's largest groundwater depression cone. Ecological Indicators, 117: 106662. DOI: 10.1016/j.ecolind.2020.106662

Cui, X., Wang, Z., Xu, N., Wu, J. and Yao, Z., 2024. A secondary modal decomposition ensemble deep learning model for groundwater level prediction using multi-data. Environmental Modelling & Software, 175: 105969. DOI: 10.1016/j.envsoft.2024.105969

Deb, K., Pratap, A., Agarwal, S. and Meyarivan, T., 2002. A fast and elitist multiobjective genetic algorithm: NSGA-II. IEEE Transactions On Evolutionary Computation, 6(2): DOI: 182-197. 10.1109/4235.996017

Deng, Y., Wang, L., Jia, H., Tong, X. and Li, F., 2019. A Sequence-to-Sequence Deep Learning Architecture Based on Bidirectional GRU for Type Recognition and Time Location of Combined Power Quality Disturbance. IEEE Transactions on Industrial Informatics, 15(8): 4481-4493. DOI: 10.1109/TII.2019.2895054.

Ding, W., Zhang, C., Lin, J., Zhao, X., Ning, Y. and Zhou, H., 2023. Flood Risk Quantification, Transmission, and Propagation Analysis for Flood Water Utilization of Parallel Reservoirs. Journal of Hydrology, 618: 129202. DOI: 10.1016/j.jhydrol.2023.129202

Fernandes, V.J., de Louw, P.G.B., Bartholomeus, R.P. and Ritsema, C.J., 2024. Machine learning for faster estimates of groundwater response to artificial aquifer recharge. Journal of Hydrology, 637: 131418. DOI: 10.1016/j.jhydrol.2024.131418

Fiori, A., de Barros, F.P.J. and Bellin, A., 2025. An Analytical Framework for Risk Evaluation and Design of Infiltration Basins for Managed Aquifer Recharge. Water Resources Research, 61(1): e2024WR038516. DOI: 10.1029/2024WR038516

Gauch, M., Kratzert, F., Klotz, D., Nearing, G., Lin, J. and Hochreiter, S., 2021. Rainfall–runoff prediction at multiple timescales with a single Long Short-Term Memory network. Hydrology and Earth System Sciences, 25(4): 2045-2062. DOI: 10.5194/hess-25-2045-2021

Guo, Z., Fogg, G. E., Chen, K., Pauloo, R. and Zheng, C., 2023. Sustainability of Regional Groundwater Quality in Response to Managed Aquifer Recharge. Water Resources Research, 59(1): e2021WR031459. DOI: DOI: 10.1029/2021WR031459

Haaf, E., Giese, M., Reimann, T. and Barthel, R., 2023. Data-Driven Estimation of Groundwater Level Time-Series at Unmonitored Sites Using Comparative Regional Analysis. Water Resources Research, 59(7): e2022WR033470. DOI: 10.1029/2022WR033470

Han, Y., Dong, Z., Cui, C., Zhang, T. and Luo, Y., 2025. Multi-objective optimization scheduling for extensive plain lake water resources incorporating flood resource utilization. Journal of Hydrology, 651: 132584. DOI: 10.1016/j.jhydrol.2024.132584

He, S., Guo, S., Zhang, J., Liu, Z., Cui, Z. and Zhang, Y. et al., 2022. Multi-objective operation of cascade reservoirs based on short-term ensemble streamflow prediction. Journal of Hydrology, 610: 127936. DOI: 10.1016/j.jhydrol.2022.127936

Hirabayashi, Y., Mahendran, R., Koirala, S., Konoshima, L., Yamazaki, D., Watanabe, S., Kim, H. and Kanae, S., 2013. Global flood risk under climate change. Nature Climate Change, 3(9): 816-821. DOI: 10.1038/nclimate1911

Hosseini, F., Prieto, C. and Alvarez, C., 2024. Hyperparameter optimization of regional hydrological LSTMs by random search: A case study from Basque Country, Spain. Journal of Hydrology, 643. DOI: 10.1016/j.jhydrol.2024.132003

Helseth, A., Mo, B., Hågenvik, H.O. and Schäffer, L.E., 2022. Hydropower Scheduling with State-Dependent Discharge Constraints: An SDDP Approach. Journal of Water Resources Planning and Management, 148(11): 04022061. DOI: 10.1061/(ASCE)WR.1943-5452.0001609

Irvine, D.J., Singha, K., Kurylyk, B.L., Briggs, M.A., Sebastian, Y., Tait, D.R. and Helton, A. M., 2024. Groundwater-Surface water interactions research: Past trends and future directions. Journal of Hydrology, 644: 132061. DOI: 10.1016/j.jhydrol.2024.132061

Jasechko, S., Seybold, H., Perrone, D., Fan, Y., Shamsudduha, M., Taylor, R.G., Fallatah, O. and Kirchner, J.W., 2024. Rapid groundwater decline and some cases of recovery in aquifers globally. Nature, 625(7996): 715-721. DOI: 10.1038/s41586-023-06879-8

Ji, X., Ding, J., Shen, H.W. and Salas, J.D., 1984. Plotting positions for Pearson type-III distribution. Journal of Hydrology, 74(1): 1-29. DOI: 10.1016/0022-1694(84)90137-9

Jain, S.K., Shilpa, L.S., Rani, D. and Sudheer, K.P., 2023. State-of-the-art review: Operation of multi-purpose reservoirs during flood season. Journal of Hydrology, 618: 129165. DOI: 10.1016/j.jhydrol.2023.129165

Jiang, Z., Liu, P., Ji, C., Zhang, H. and Chen, Y., 2019. Ecological flow considered multi-objective storage energy operation chart optimization of large-scale mixed reservoirs. Journal of Hydrology, 577: 123949. DOI: 10.1016/j.jhydrol.2019.123949

Kuang, X.X., Liu, J.G., Scanlon, B.R., Jiao, J.J., Jasechko, S. and Lancia, M.et al., 2024. The changing nature of groundwater in the global water cycle. Science, 383(6686). DOI: 10.1126/science.adf0630

Li, J., Zhang, W. and Yeh, W.W.G., 2021. A Proposed Multi-Objective, Multi-Stage Stochastic Programming with Recourse Model for Reservoir Management and Operation. Water Resources Research, 57(10): e2020WR029200. DOI: 10.1029/2020WR029200

Liu, P., Li, L., Guo, S., Xiong, L., Zhang, W., Zhang, J. and Xu, C., 2015. Optimal design of seasonal flood limited water levels and its application for the Three Gorges Reservoir. Journal of Hydrology, 527: 1045-1053. DOI: 10.1016/j.jhydrol.2015.05.055

Lyu, K., Dong, Y., Lyu, W., Zhou, Y., Wang, S., Wang, Z., Cui, W., Zhang, Y., Zhang, Q. and Cui, Y., 2025. Data-driven and numerical simulation coupling to quantify the impact of ecological water replenishment on surface water-groundwater interactions. Journal of Hydrology, 649: 132508. DOI: 10.1016/j.jhydrol.2024.132508

Malhotra, P., Ramakrishnan, A., Anand, G., Vig, L., Agarwal, P. and Shroff, G.M., 2016. LSTM-based Encoder-Decoder for Multi-sensor Anomaly Detection. Arxiv Preprint Arxiv:1607.00148. DOI:10.48550/arXiv.1607.00148

Mateo, C. M., Hanasaki, N., Komori, D., Tanaka, K., Kiguchi, M., Champathong, A., Sukhapunnaphan, T., Yamazaki, D. and Oki, T., 2014. Assessing the impacts of reservoir operation to floodplain inundation by combining hydrological, reservoir management, and hydrodynamic models. Water Resources Research, 50(9): 7245-7266. DOI: 10.1002/2013WR014845

Mu, Z.Y., Ai, X.S., Ding, J., Huang, K., Chen, S.L., Guo, J.J. and Dong, Z., 2022. Risk Analysis of Dynamic Water Level Setting of Reservoir in Flood Season Based on Multi-index.

Water Resources Management, 36(9): 3067-3086. DOI: 10.1007/s11269-022-03188-z

Page, D., Vanderzalm, J., Miotliński, K., Barry, K., Dillon, P., Lawrie, K., et al., 2014. Determining treatment requirements for turbid river water to avoid clogging of aquifer storage and recovery wells in siliceous alluvium. Water Research, 66:99-110. DOI: 10.1016/j.watres.2014.08.018

Rodríguez, E., P., Canelles, A., Sanchez-Vila, X., Folch, A., Kurtzman, D., Rossetto, R., et al., 2018. A risk assessment methodology to evaluate the risk failure of managed aquifer recharge in the Mediterranean Basin. Hydrology and Earth System Sciences, 22(6): 3213-3227. DOI: 10.5194/hess-22-3213-2018

Owuor, S.O., Butterbach-Bahl, K., Guzha, A.C., Rufino, M.C., Pelster, D.E., Díaz-Pinés, E. and Breuer, L., 2016. Groundwater recharge rates and surface runoff response to land use and land cover changes in semi-arid environments. Ecological Processes, 5(1): 16. DOI: 10.1186/s13717-016-0060-6

Roy, D.K., Leslie, D.L., Reba, M.L., Hashem, A.A., Bellis, E. and Nowlin, J., 2024. Optimizing the quantity of recharge water into a sedimentary aquifer through infiltration galleries using a surrogate assisted coupled simulation–optimization approach. Journal of Hydrology, 635: 131183. DOI:10.1016/j.jhydrol.2024.131183

Hochreiter, S. and Schmidhuber, J., 1997. Long Short-Term Memory. Neural Computation, 9(8): 1735-1780. DOI: 10.1162/neco.1997.9.8.1735.

Verma, S., Pant, M. and Snasel, V. 2021. A Comprehensive Review on NSGA-II for Multi-Objective Combinatorial Optimization Problems. IEEE Access, 9: 57757-57791. DOI: 10.1109/ACCESS.2021.3070634

Samanta, S., Sheng, Z., Munster, C.L. and Van Houtte, E., 2020. Seasonal variation of infiltration rates through pond bed in a managed aquifer recharge system in St-André, Belgium. Hydrological Processes, 34(18): 3807-3823. DOI: 10.1002/hyp.13827

Schäffer, L.E., Helseth, A. and Korpas, M., 2022. A stochastic dynamic programming model for hydropower scheduling with state-dependent maximum discharge constraints. Renewable Energy, 194: 571-581. DOI: 10.1016/j.renene.2022.05.106

Solgi, R., Loáiciga, H. A. and Kram, M., 2021. Long short-term memory neural network (LSTM-NN) for aquifer level time series forecasting using in-situ piezometric observations. Journal of Hydrology, 601: 126800. DOI: 10.1016/j.jhydrol.2021.126800

Sutskever I., Vinyals, O. and Le, Q.V., 2014. Sequence to Sequence Learning with Neural Networks. Arxiv E-Prints: arXiv:1409.3215. DOI: 10.48550/arXiv.1409.3215Tabari, H., 2020. Climate change impact on flood and extreme precipitation increases with water availability. Scientific Reports, 10(1): 13768. DOI: 10.1038/s41598-020-70816-2

Tang, W., Zhao, X., Wang, J., Motagh, M., Xu, H., Ru, Z. and Wang, Y., 2024. Land surface response to groundwater drawdown and recovery in Taiyuan city, Northern China, analyzed with a long-term elevation change measurements from leveling and multi-sensor InSAR. Journal of Hydrology, 641: 131781. DOI: 10.1016/j.jhydrol.2024.131781

Tennant, D.L., 1976. Instream Flow Regimens for Fish, Wildlife, Recreation and Related Environmental Resources. Fisheries, 1(4): 6-10. DOI: 10.1577/1548-8446(1976) 001<0006: IFRFFW>2.0.CO;2

Tripathy, K.P. and Mishra, A.K., 2024. Deep learning in hydrology and water resources disciplines: concepts, methods, applications, and research directions. Journal of Hydrology, 628: 130458. DOI: 10.1016/j.jhydrol.2023.130458

Wang, K., Wang, Z., Liu, K., Du, H., Mo, Y., Wang, M., Jin, G. and Li, L., 2022. Assessing the floodwater utilization potential in a reservoir-controlled watershed: A novel method considering engineering regulations and an empirical case from China. Ecological Informatics, 68: 101581. DOI: 10.1016/j.ecoinf.2022.101581

Wang, K., Wang, Z.Z., Xu, J., Mo, Y.M., Cheng, L., Bai, Y., Du, H.H. and Liu, K.L., 2023. Floodwater utilization potential assessment of China based on improved conceptual model and multi-reservoir basin assessment method. Journal of Hydrology, 625. DOI: 10.1016/j.jhydrol.2023.129921

Wei, G., Liang, G., Ding, W., He, B., Wu, J., Ren, M. and Zhou, H., 2022. Deriving optimal operating rules for flood control considering pre-release based on forecast information. Journal of Hydrology, 615: 128665. DOI: 10.1016/j.jhydrol.2022.128665

Wunsch, A., Liesch, T. and Broda, S., 2021. Groundwater level forecasting with artificial neural networks: a comparison of long short-term memory (LSTM), convolutional neural networks (CNNs), and non-linear autoregressive networks with exogenous input (NARX). Hydrology and Earth System Sciences, 25(3): 1671-1687. DOI: 10.5194/hess-25-1671-2021

Xiang, Z., Yan, J. and Demir, I., 2020. A Rainfall-Runoff Model With LSTM-Based Sequence-to-Sequence Learning. Water Resources Research, 56(1): e2019WR025326. DOI: 10.1029/2019WR025326

Yang, G., Guo, S., Liu, P., Li, L. and Xu, C., 2017. Multiobjective reservoir operating rules based on cascade reservoir input variable selection method. Water Resources Research, 53(4): 3446-3463. DOI: 10.1002/2016WR020301

Yang, S., Zhao, B., Yang, D., Wang, T., Yang, Y., Ma, T. and Santisirisomboon, J., 2023. Future changes in water resources, floods and droughts under the joint impact of climate and land-use changes in the Chao Phraya basin, Thailand. Journal of Hydrology, 620: 129454. DOI: 10.1016/j.jhydrol.2023.129454

Zhang, C., Duan, Q. Y., Yeh, P. J. F., Pan, Y., Gong, H. L., Gong, W., Di, Z., Lei, X., Liao, W., Huang, Z., Zheng, L. and Guo, X., 2020. The Effectiveness of the South-to-North Water Diversion Middle Route Project on Water Delivery and Groundwater Recovery in North China Plain. Water Resources Research, 56(10): e2019WR026759. DOI: 10.1029/2019WR026759

Zhuang, D., Gan, V.J.L., Tekler, Z.D., Chong, A.D., Tian, S. and Shi, X., 2023. Data-driven predictive control for smart HVAC system in IoT-integrated buildings with time-series forecasting and reinforcement learning. Applied Energy, 338. DOI: 10.1016/j.apenergy.2023.120936